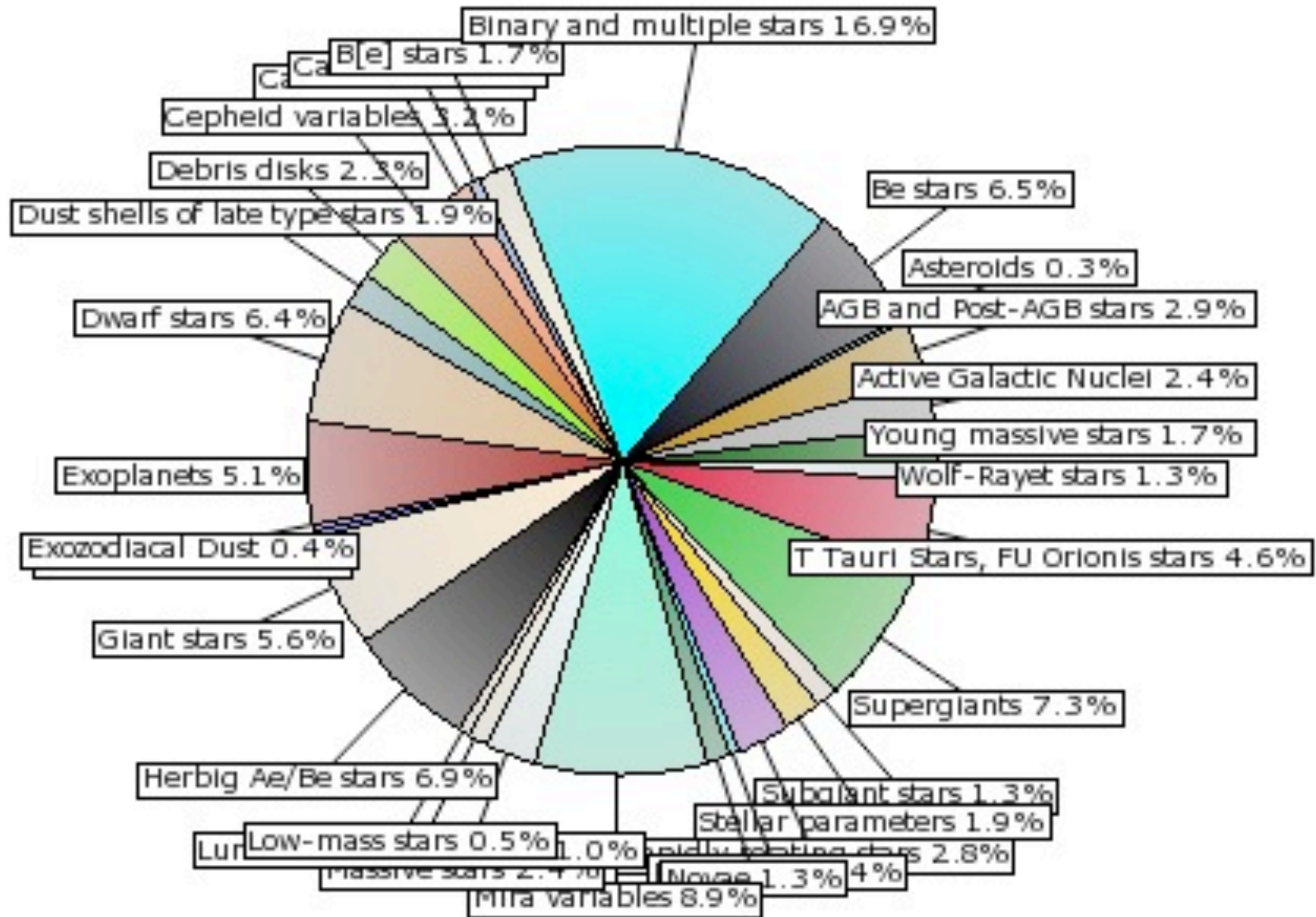


# Binaries as seen by Optical Long Baseline Interferometry

[jean-baptiste.lebouquin@obs.ujf-grenoble.fr](mailto:jean-baptiste.lebouquin@obs.ujf-grenoble.fr)

IPAG - Grenoble  
PI of the PIONIER instrument

# Remember: binaries are the workhorse of OLBIN

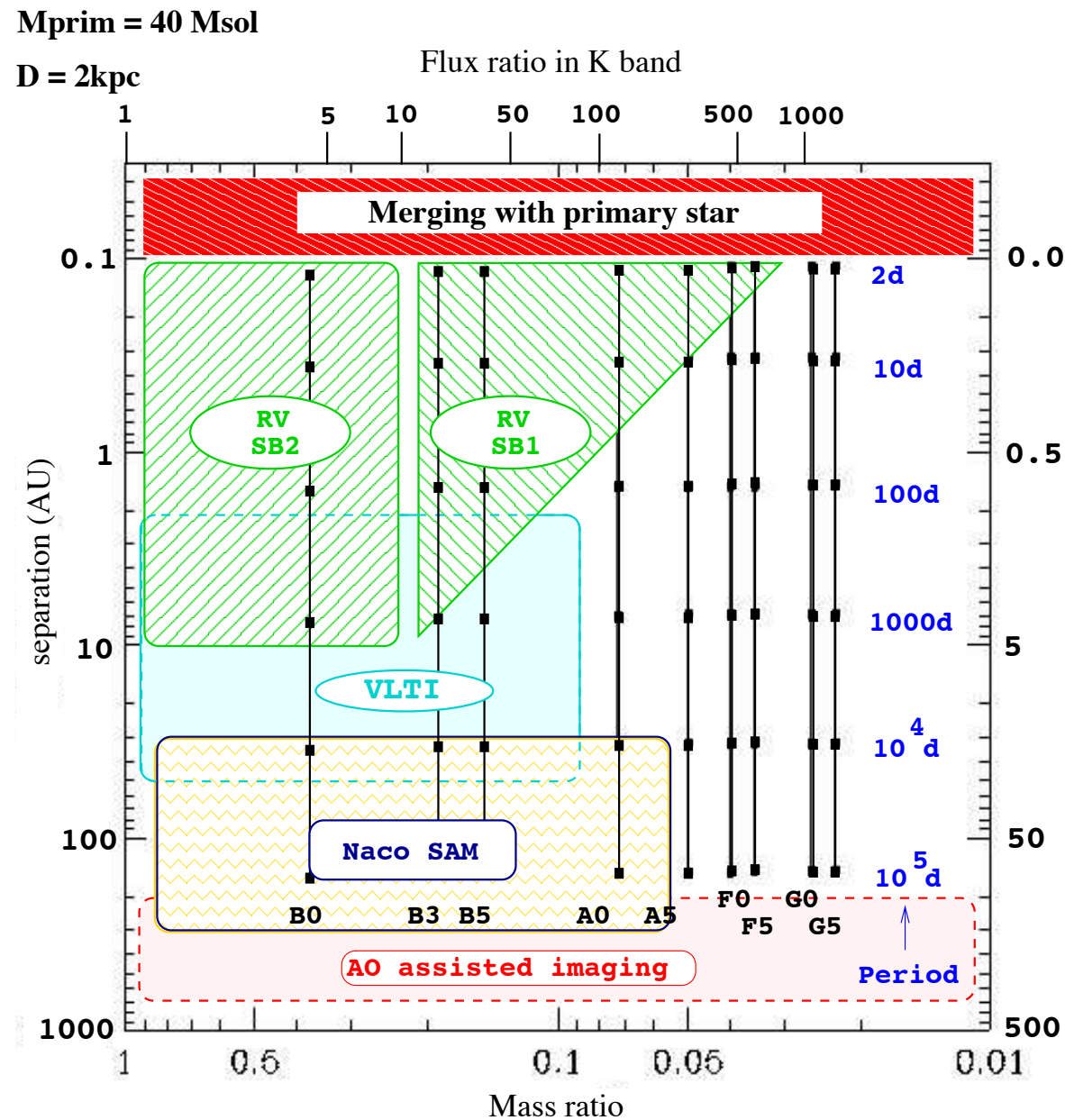


plot made with <http://apps.jmmc.fr/bibdb/>

# Astrophysical topics covered by “binary”

- **Multiplicity (complement RV + AO)**
  - Massive stars, young stars, active stars
  - Faint companions, low mass stars and planets
- **Dynamical masses (SB2 + astrometry)**
  - All stars (massive, low mass, young, old, MS...)
- **Shaping of environment**
  - Evolved stars: shaping of PN and disk
  - Young stars: shaping of proto-planetary disk
  - Be stars: relation with the disk (generation, distortion, dissipation...)
- **Interacting binaries**
  - Evolved stars: mass transfer
  - Massive stars: wind-wind collision, X-ray emitters

# Multiplicity: large surveys



## Survey of massive stars at high angular resolution

### I. PIONIER/VLTI observations of hundred O-stars\*

H. Sana<sup>2</sup>, S. Lacour<sup>3</sup>, J.-B. Le Bouquin<sup>1</sup>, G. Duvert<sup>1</sup>, J.-P. Berger<sup>4</sup>, O. Absil<sup>5, \*\*</sup>, and G. Zins<sup>1</sup>

- <sup>1</sup> UJF-Grenoble 1 / CNRS-INSU, Institut de Planétologie et d'Astrophysique de Grenoble (IPAG) UMR 5274, Grenoble, France  
<sup>2</sup> Astronomical Institute Anton Pannekoek, Amsterdam University, Science Park 904, 1098 XH, Amsterdam, The Netherlands  
<sup>3</sup> Observatoire de Paris, 5 place Jules Janssen, Meudon, France  
<sup>4</sup> European Southern Observatory, Karl-Schwarzschild-Str. 2, 85748, Garching bei München, Germany  
<sup>5</sup> Institut d'Astrophysique et de Géophysique, Université de Liège, 17 Allée du Six Août, B-4000 Liège, Belgium

in preparation

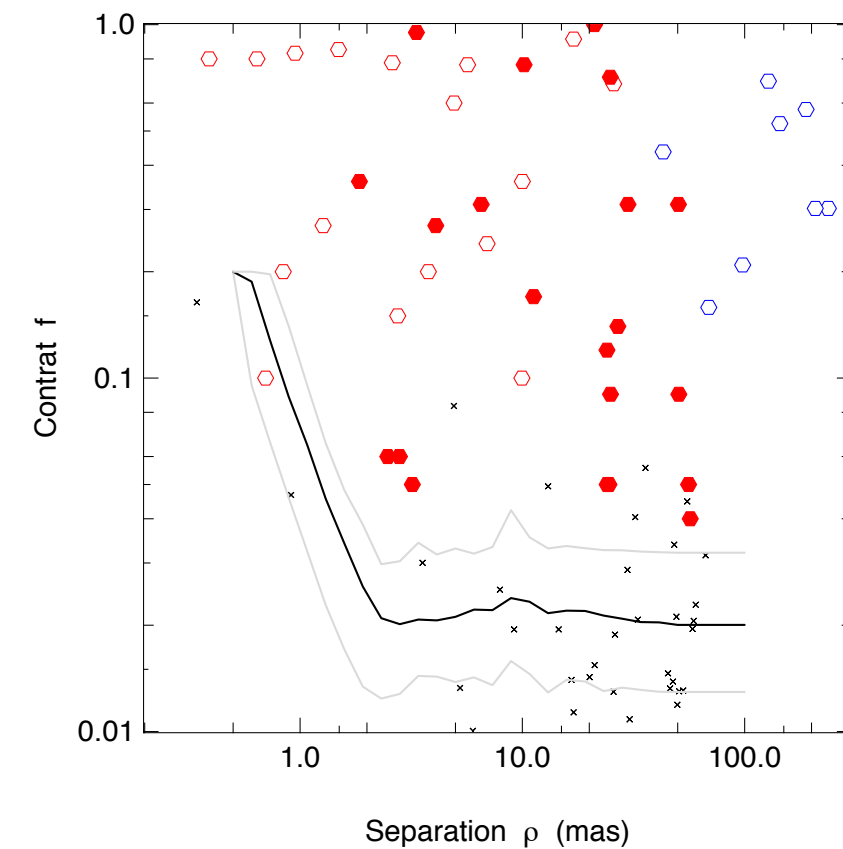
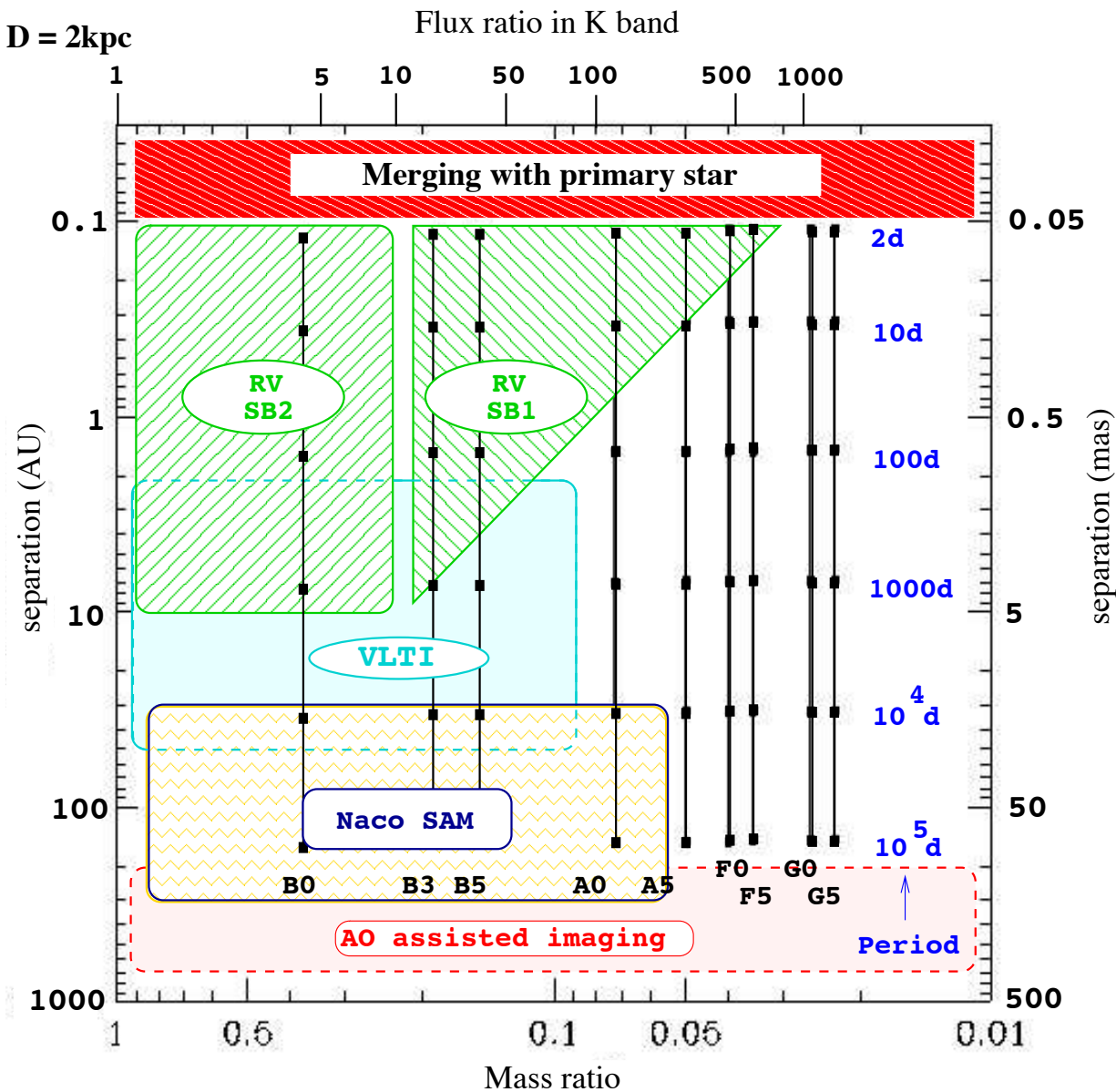


**Fig. 4.** Plot of separation ( $\rho$ ) in milli-arcsecond vs. flux ratio ( $f$ ) for pairs observed. The filled red symbols represent the pairs discovered in this survey. The open red symbols are objects for which we probably spatially resolved for the first time a known SB pair. The open blue symbols are the pairs already resolved by Mason et al. (2009) with single-dish observation. The solid lines indicate the median sensitivity of our survey and its typical variation between the objects.

# Multiplicity and faint companion

$M_{\text{prim}} = 40 M_{\text{sol}}$

$D = 2 \text{ kpc}$



## Deep near-infrared interferometric search for low-mass companions around $\beta$ Pictoris<sup>\*</sup>

O. Absil<sup>1, \*\*</sup>, J.-B. Le Bouquin<sup>2</sup>, J. Lebreton<sup>2</sup>, J.-C. Augereau<sup>2</sup>, M. Benisty<sup>3</sup>, G. Chauvin<sup>2</sup>, C. Hanot<sup>1</sup>, A. Mérand<sup>4</sup>, and G. Montagnier<sup>4</sup>

<sup>1</sup> Institut d'Astrophysique et de Géophysique, Université de Liège, 17 Allée du Six Août, 4000 Liège, Belgium

e-mail: absil@astro.ulg.ac.be

<sup>2</sup> LAOG-UMR 5571, CNRS and Université Joseph Fourier, BP 53, 38041 Grenoble, France

<sup>3</sup> INAF - Osservatorio Astrofisico di Arcetri, Largo E. Fermi 5, 50125 Firenze, Italy

<sup>4</sup> European Southern Observatory, Casilla 19001, Santiago 19, Chile

Received 4 June 2010 / Accepted 3 September 2010

### ABSTRACT

**Aims.** We search for low-mass companions in the innermost region ( $< 300 \text{ mas}$ , i.e.,  $6 \text{ AU}$ ) of the  $\beta$  Pic planetary system.

**Methods.** We obtained interferometric closure phase measurements in the  $K$ -band with the VLTI/AMBER instrument used in its medium spectral resolution mode. Fringe stabilization was provided by the FINITO fringe tracker.

**Results.** In a search region of between  $2$  and  $60 \text{ mas}$  in radius, our observations exclude at  $3\sigma$  significance the presence of companions with  $K$ -band contrasts greater than  $5 \times 10^{-3}$  for  $90\%$  of the possible positions in the search zone (i.e.,  $90\%$  completeness). The median  $1\sigma$  error bar in the contrast of potential companions within our search region is  $1.2 \times 10^{-3}$ . The best fit to our data set using a binary model is found for a faint companion located at about  $14.4 \text{ mas}$  from  $\beta$  Pic, which has a contrast of  $1.8 \times 10^{-3} \pm 1.1 \times 10^{-3}$  (a result consistent with the absence of companions). For angular separations larger than  $60 \text{ mas}$ , both time smearing and field-of-view limitations reduce the sensitivity.

**Conclusions.** We can exclude the presence of brown dwarfs with masses higher than  $29 M_{\text{Jup}}$  (resp.  $47 M_{\text{Jup}}$ ) at a  $50\%$  (resp.  $90\%$ ) completeness level within the first few AU around  $\beta$  Pic. Interferometric closure phases offer a promising way to directly image low-mass companions in the close environment of nearby young stars.

**Key words.** stars: individual:  $\beta$  Pic – planets and satellites: detection – techniques: interferometric – planetary systems

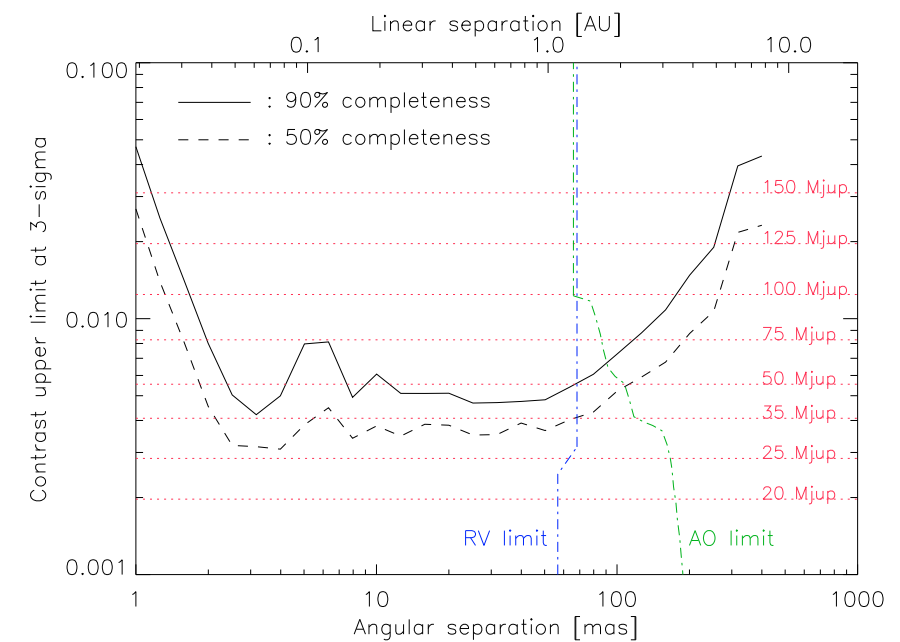


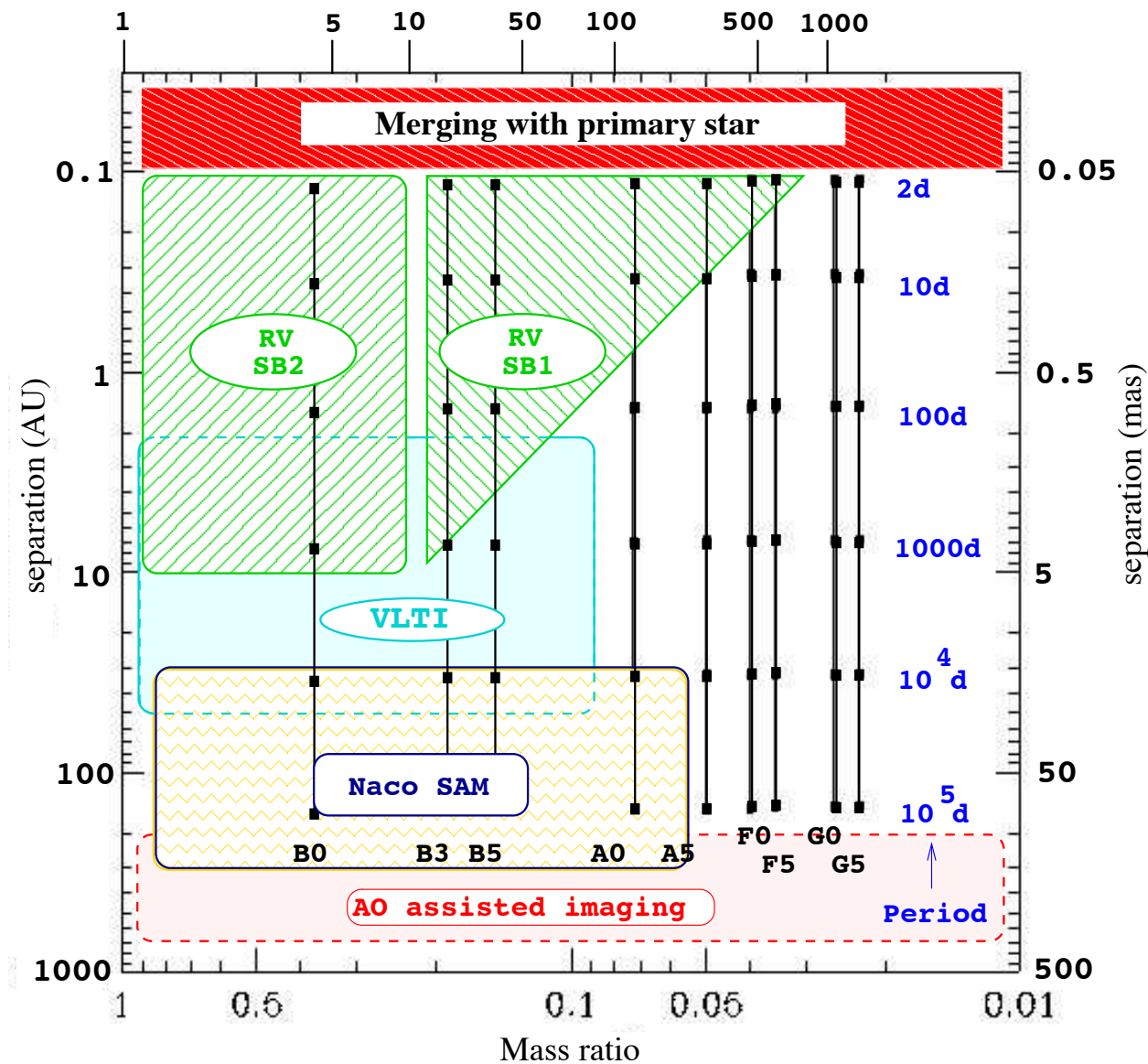
**Fig. 4.** Sensitivity curves showing the  $3\sigma$  upper limit to the contrast of off-axis companions as a function of the angular separation for  $50\%$  and  $90\%$  completeness, computed across annular fields-of-view with  $10\%$  relative width. Equivalent masses were computed using the COND model of Baraffe et al. (2003), for an age of  $12 \text{ Myr}$ . The companion dis-

# Measuring stellar masses and distance

$M_{\text{prim}} = 40 M_{\odot}$

$D = 2 \text{ kpc}$

Flux ratio in K band



Astronomy & Astrophysics manuscript no. zetaori  
June 4, 2013

© ESO 2013

## Dynamical mass of the O-type supergiant in Zeta Orionis A<sup>\*</sup>

C.A. Hummel<sup>1</sup>, Th. Rivinius<sup>2</sup>, M.-F. Nieva<sup>3,4</sup>, O. Stahl<sup>5</sup>, G. van Belle<sup>6</sup>, and R.T. Zavala<sup>7</sup>

<sup>1</sup> European Southern Observatory, Karl-Schwarzschild-Str. 2, 85748 Garching \*\*

<sup>2</sup> European Southern Observatory, Casilla 19001, Santiago 19, Chile

<sup>3</sup> Dr. Karl Remeis-Sternwarte & ECAP, University of Erlangen-Nuremberg, Sternwartstr. 7, 96049 Bamberg

<sup>4</sup> Institute of Astro- and Particle Physics, University of Innsbruck, Technikerstr. 25, 6020 Innsbruck, Austria

<sup>5</sup> ZAH, Landessternwarte Heidelberg-Königstuhl, 69117 Heidelberg

<sup>6</sup> Lowell Observatory, 1400 W. Mars Hill Rd., Flagstaff, AZ 86001, USA

<sup>7</sup> U.S. Naval Observatory, Flagstaff Station, 10391 W. Naval Obs. Rd., Flagstaff, AZ 86001, USA

Received: <date>; accepted: <date>; L<sup>A</sup>T<sub>E</sub>Xed: June 4, 2013

### ABSTRACT

**Aims.** A close companion of  $\zeta$  Orionis A was found in 2000 with the Navy Precision Optical Interferometer (NPOI), and shown to be a physical companion. Because the primary is a supergiant of type O, for which dynamical mass measurements are very rare, the companion was observed with NPOI over the full 7-year orbit. Our aim was to determine the dynamical mass of a supergiant that, due to the physical separation of more than 10 AU between the components, cannot have undergone mass exchange with the companion.

**Methods.** The interferometric observations allow measuring the relative positions of the binary components and their relative brightness. The data collected over the full orbital period allows all seven orbital elements to be determined. In addition to the interferometric observations, we have analyzed archival spectra obtained at the Calar Alto, Haute Provence, Cerro Armazones, and La Silla observatories, as well as new spectra obtained at the VLT on Cerro Paranal. In the high-resolution spectra we identified a few lines that can be associated exclusively to one or the other component for the measurement of the radial velocities of both. The combination of astrometry and spectroscopy then yields the stellar masses and the distance to the binary star.

**Results.** The resulting masses for components Aa of  $14.0 \pm 2.2 M_{\odot}$  and Ab of  $7.4 \pm 1.1 M_{\odot}$  are low compared to theoretical expectations, with a distance of  $294 \pm 21$  pc which is smaller than a photometric distance estimate of  $387 \pm 54$  pc based on the spectral type B0III of the B component. If the latter (because it is also consistent with the distance to the Orion OB1 association) is adopted, the mass of the secondary component Ab of  $14 \pm 3 M_{\odot}$  would agree with classifying a star of type B0.5IV. It is fainter than the primary by about  $2.2 \pm 0.1$  magnitudes in the visual. The primary mass is then determined to be  $33 \pm 10 M_{\odot}$ . The possible reasons for the distance discrepancy are most likely related to physical effects, such as small systematic errors in the radial velocities due to stellar winds.

**Key words.** techniques: interferometric - binaries: spectroscopic - stars: supergiants - stars: fundamental parameters - stars: individual: Zeta Orionis A

# From observations to stellar masses

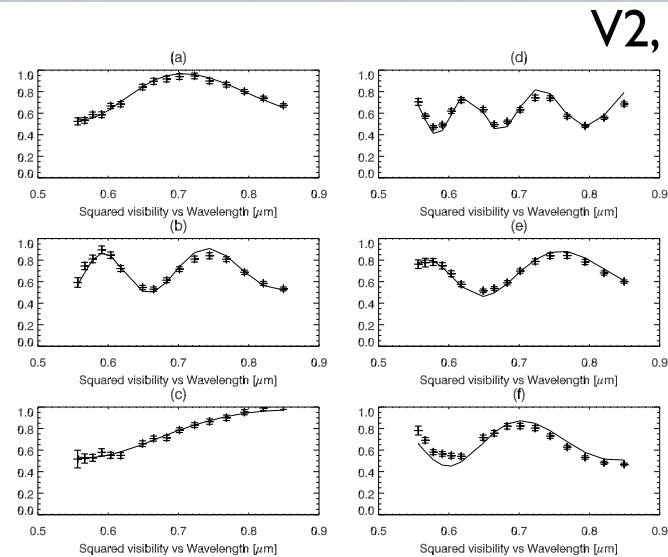


**Fig. 1.** Calibrated (squared) visibility amplitudes plotted versus wavelength for 2002 Dec 20 on the E-E2(a), E2-W(b), E2-N(c), E-W(d), E-N(e), and N-W(f) baselines at 7:45 UT. The solid line shows the model prediction for a fit with component separation  $\rho = 24.6$  mas and PA  $\theta = 87.7^\circ$ . The amplitude of the quasi-sinusoidal amplitude variation is fit with a magnitude difference  $\Delta m = 2.2$ .

V2, t3Phi

Relative position on sky

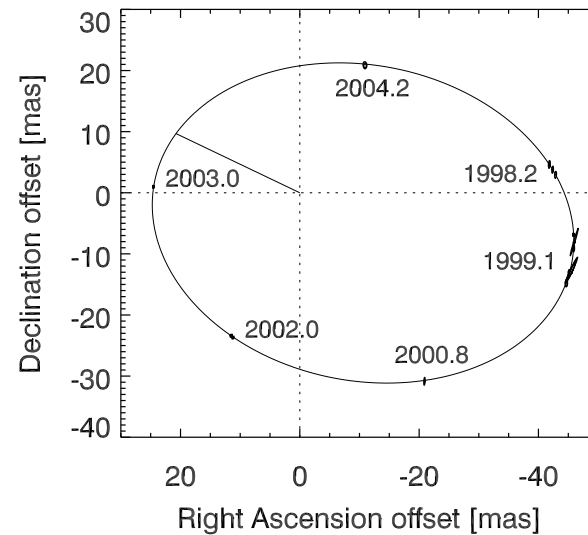


**Fig. 4.** Orbit of  $\zeta$  Orionis Ab around Aa (center). The line indicates the secondary Ab at periastron. A few selected epochs are marked.

True masses and distance

**Table 3.** Orbital elements and system parameters

Orbital period	$2687.3 \pm 7.0$ d
Periastron epoch	JD $2452734.2 \pm 9.0$
Periastron long.	$24.2 \pm 1.2^\circ$
Eccentricity	$0.338 \pm 0.004$
Ascending node	$83.8 \pm 0.8^\circ$
Inclination	$139.3 \pm 0.6^\circ$
Semi-major axis	$35.9 \pm 0.2$ mas
Systemic velocity	$28.3 \pm 0.5$ km/s
Orbital parallax	$3.4 \pm 0.2$ mas
Visual magnitude difference	$2.2 \pm 0.1$
$M_{Aa}$	$14.0 \pm 2.2 M_\odot$
$M_{Ab}$	$7.4 \pm 1.1 M_\odot$
$K_1$ (derived)	10.1 km/s
$K_2$ (derived)	19.6 km/s

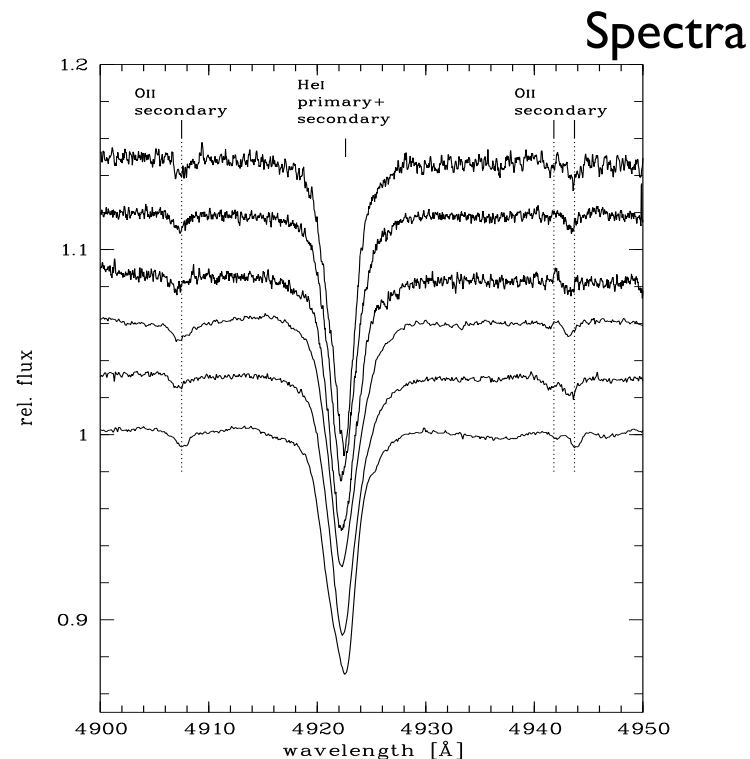


**Fig. 3.** The SB2 composite spectrum of  $\zeta$  Ori Aa+Ab. The panel shows the weak O II 4943 lines from the secondary and the composite He I 4922 line. The three HEROS and three FEROS spec-

Spectra

Radial velocities

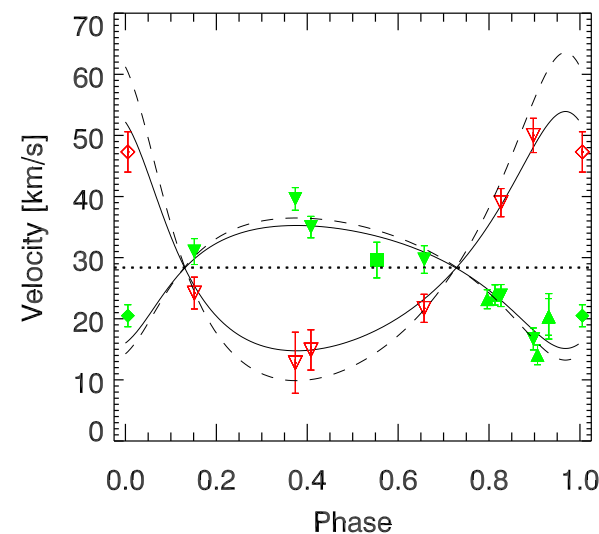


**Fig. 5.** The measured RVs of both components. The green (filled) symbols denote the primary (He II 4542), the red (open) symbols the secondary (O II 4943). Triangles pointing down denote FEROS/HEROS measurements, triangles pointing up denote BESO. Squares denote ELODIE, and the diamond is for UVES. The dashed lines are for the model based on the photometric distance (see discussion; the derived velocity semi-amplitudes are  $K_1 = 11.6$  km/s and  $K_2 = 26.8$  km/s).

# Interacting binaries

## FIRST RESOLVED IMAGES OF THE ECLIPSING AND INTERACTING BINARY $\beta$ LYRAE

M. ZHAO,<sup>1</sup> D. GIES,<sup>2</sup> J. D. MONNIER,<sup>1</sup> N. THUREAU,<sup>3</sup> E. PEDRETTI,<sup>3</sup> F. BARON,<sup>4</sup> A. MERAND,<sup>2</sup> T. TEN BRUMMELAAR,<sup>2</sup> H. MCALISTER,<sup>2</sup> S. T. RIDGWAY,<sup>5</sup> N. TURNER,<sup>2</sup> J. STURMANN,<sup>2</sup> L. STURMANN,<sup>2</sup> C. FARRINGTON,<sup>2</sup> AND P. J. GOLDFINGER<sup>2</sup>

Received 2008 May 5; accepted 2008 July 28; published 2008 August 21

### ABSTRACT

We present the first resolved images of the eclipsing binary  $\beta$  Lyrae, obtained with the CHARA Array interferometer and the MIRC combiner in the  $H$  band. The images clearly show the mass donor and the thick disk surrounding the mass gainer at all six epochs of observation. The donor is brighter and generally appears elongated in the images, the first direct detection of photospheric tidal distortion due to Roche lobe filling. We also confirm expectations that the disk component is more elongated than the donor and is relatively fainter at this wavelength. Image analysis and model fitting for each epoch were used for calculating the first astrometric orbital solution for  $\beta$  Lyrae, yielding precise values for the orbital inclination and position angle. The derived semimajor axis also allows us to estimate the distance of  $\beta$  Lyrae; however, systematic differences between the models and the images limit the accuracy of our distance estimate to about 15%. To address these issues, we will need a more physical, self-consistent model to account for all epochs as well as the multiwavelength information from the eclipsing light curves.

*Subject headings:* binaries: eclipsing — infrared: stars — stars: fundamental parameters — stars: individual ( $\beta$  Lyrae) — techniques: interferometric

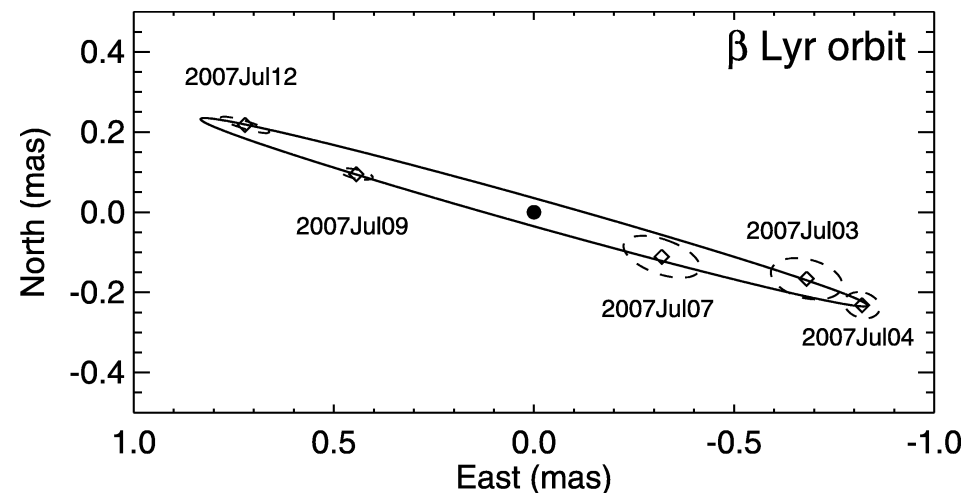
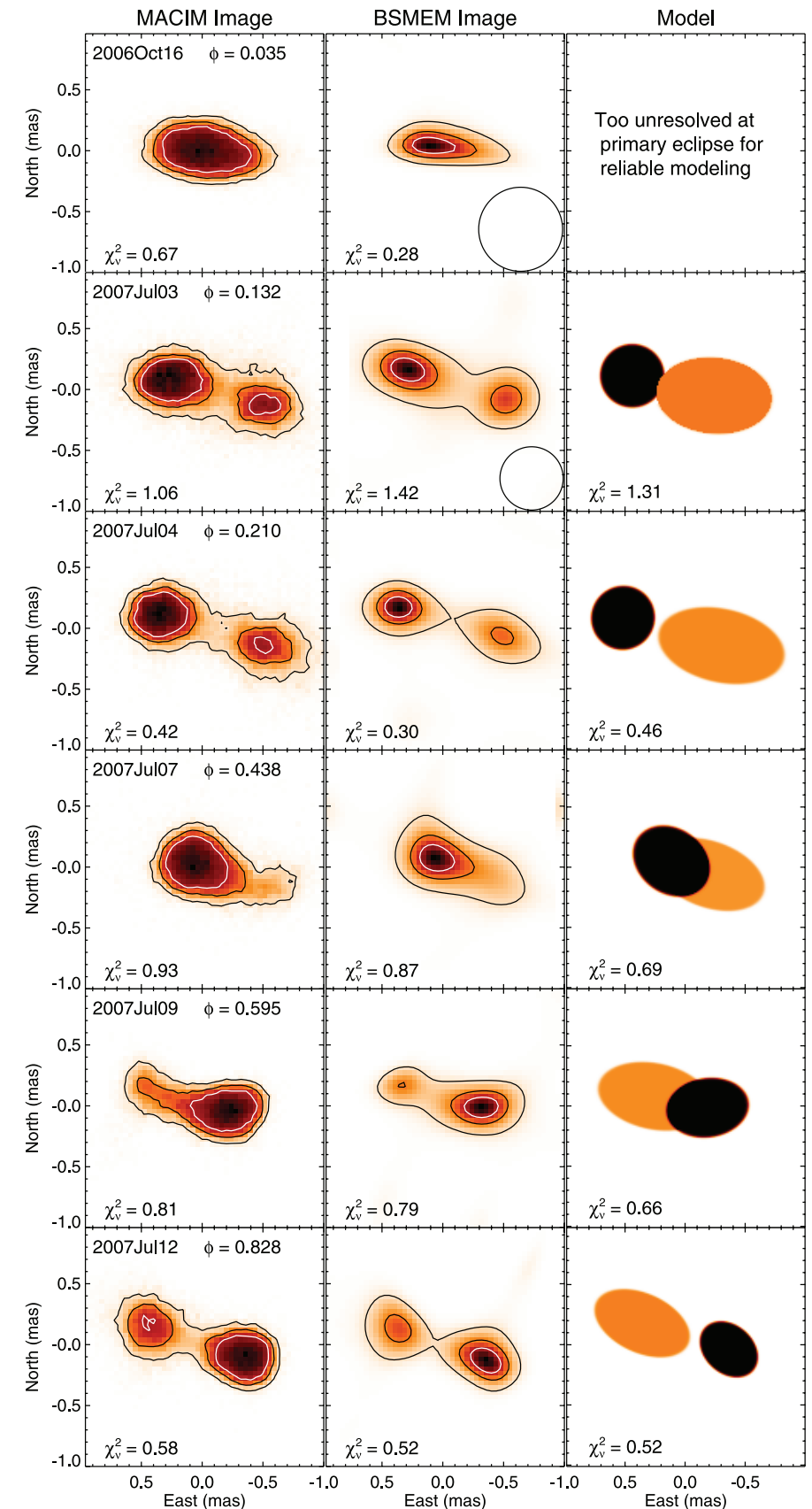


FIG. 3.—The best-fit relative orbit of  $\beta$  Lyr (solid line). The donor is indicated as a filled dot in the center. Positions of each epoch are shown by the open dots, surrounded by their error ellipses in dashed lines. The upper part of the orbit is located toward the observer.



# Interacting binaries

## An incisive look at the symbiotic star SS Leporis

### Milli-arcsecond imaging with PIONIER/VLTI<sup>\*,\*\*</sup>

N. Blind<sup>1</sup>, H. M. J. Boffin<sup>2</sup>, J.-P. Berger<sup>2</sup>, J.-B. Le Bouquin<sup>1</sup>, A. Mérand<sup>2</sup>, B. Lazareff<sup>1</sup>, and G. Zins<sup>1</sup>

<sup>1</sup> UJF-Grenoble 1/CNRS-INSU, Institut de Planétologie et d'Astrophysique de Grenoble (IPAG) UMR 5274, Grenoble, France

e-mail: nicolas.blind@obs.ujf-grenoble.fr

<sup>2</sup> European Southern Observatory, Casilla 19001, Santiago 19, Chile

e-mail: hboffin@eso.org

Received 7 September 2011 / Accepted 20 November 2011

#### ABSTRACT

**Context.** Determining the mass transfer in a close binary system is of prime importance for understanding its evolution. SS Leporis, a symbiotic star showing the Algol paradox and presenting clear evidence of ongoing mass transfer, in which the donor has been thought to fill its Roche lobe, is a target particularly suited to this kind of study.

**Aims.** Since previous spectroscopic and interferometric observations have not been able to fully constrain the system morphology and characteristics, we go one step further to determine its orbital parameters, for which we need new interferometric observations directly probing the inner parts of the system with a much higher number of spatial frequencies.

**Methods.** We use data obtained at eight different epochs with the VLTI instruments AMBER and PIONIER in the *H* and *K* bands. We performed aperture synthesis imaging to obtain the first model-independent view of this system. We then modelled it as a binary (whose giant is spatially resolved) that is surrounded by a circumbinary disc.

**Results.** Combining these interferometric measurements with previous radial velocities, we fully constrain the orbit of the system. We then determine the mass of each star and significantly revise the mass ratio. The M giant also appears to be almost twice smaller than previously thought. Additionally, the low spectral resolution of the data allows the flux of both stars and of the dusty disc to be determined along the *H* and *K* bands, and thereby extracting their temperatures.

**Conclusions.** We find that the M giant actually does not *stricto sensu* fill its Roche lobe. The mass transfer is more likely to occur through the accretion of an important part of the giant wind. We finally raise the possibility for an enhanced mass loss from the giant, and we show that an accretion disc should have formed around the A star.

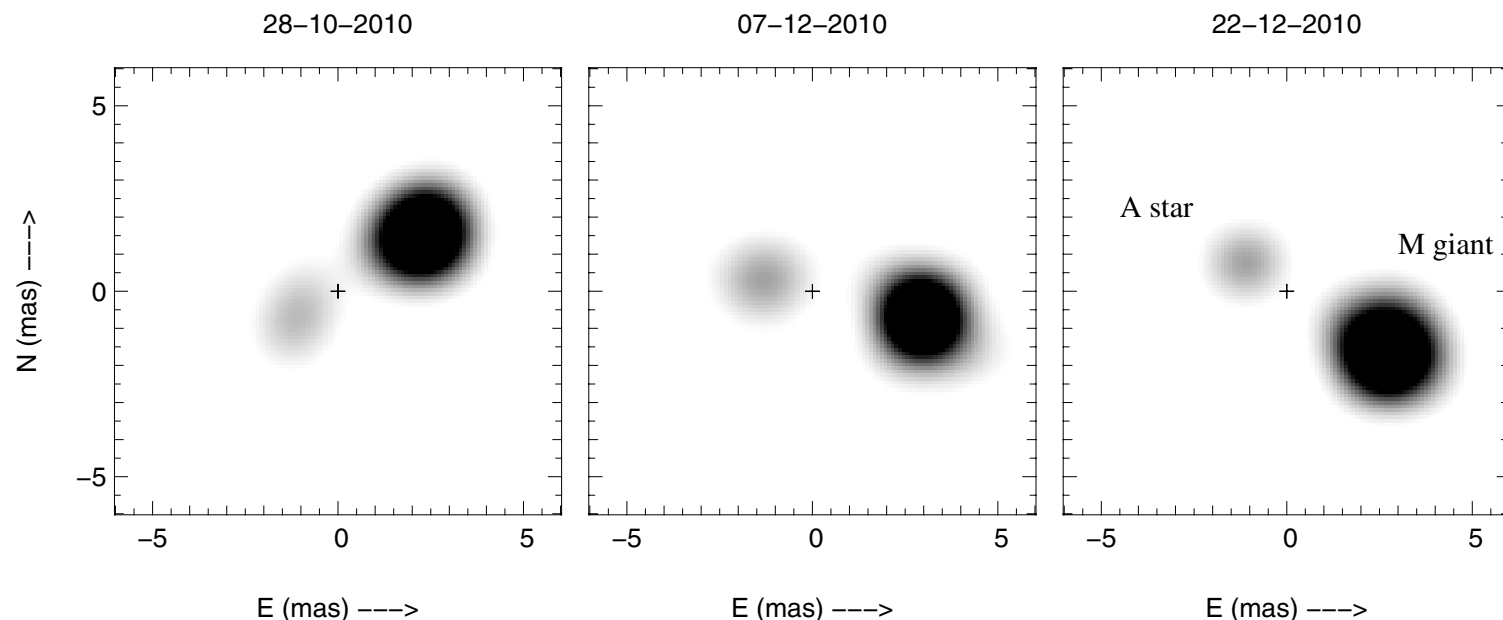


**Fig. 2.** Model-independent image reconstruction of SS Lep obtained during the PIONIER runs P1, P2, and P4. The resolved M giant and the A star are clearly identified. The images are centered on the center of mass (central cross) as determined from Sect. 5.2. The distortion of the giant in the image is most certainly due to an asymmetric PSF rather than to a definite tidal effect. Three faint artefacts are visible on the periphery of the image.

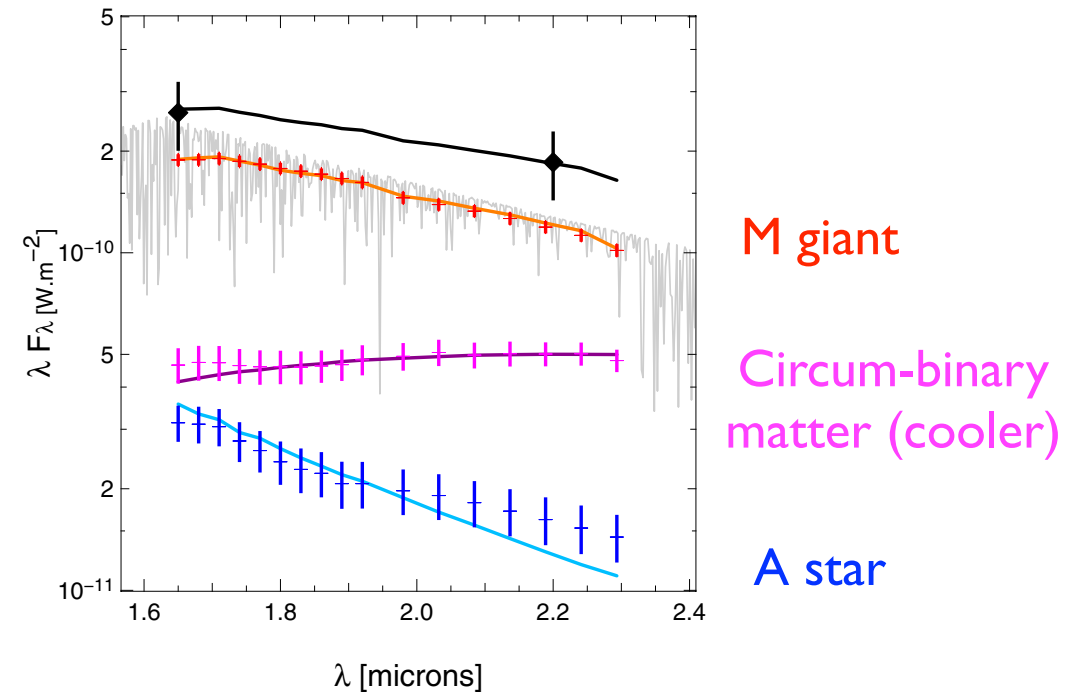


**Fig. 4.** Flux of the M giant (red), the A star (blue), and the envelope (magenta). The grey curve is the M star MARCS spectrum. In black is the sum of the three components adjusted to the 2MASS magnitudes in the *H*- and *K*-bands. The dots are the data plus the error bars, and the solid lines are the models for each of the components.

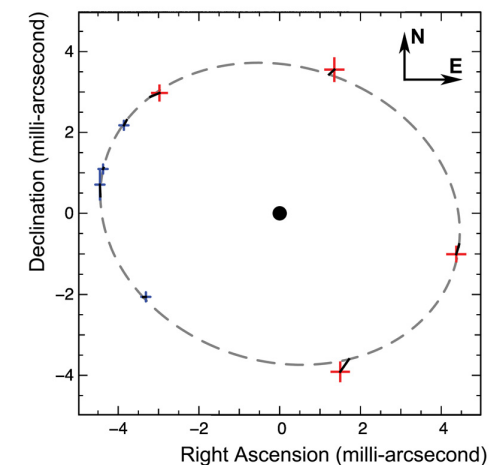


**Fig. 3.** SS Lep best orbit (dashed line) obtained by combining previous radial velocities (Welty & Wade 1995) with our astrometric measurements. The central dot indicates the A star. AMBER and PIONIER points are respectively presented by the red and blue crosses representing the 3- $\sigma$  error bars. The corresponding points on the best orbit are indicated by the short segments originating in each point.

# Formulation of a binary in visibility

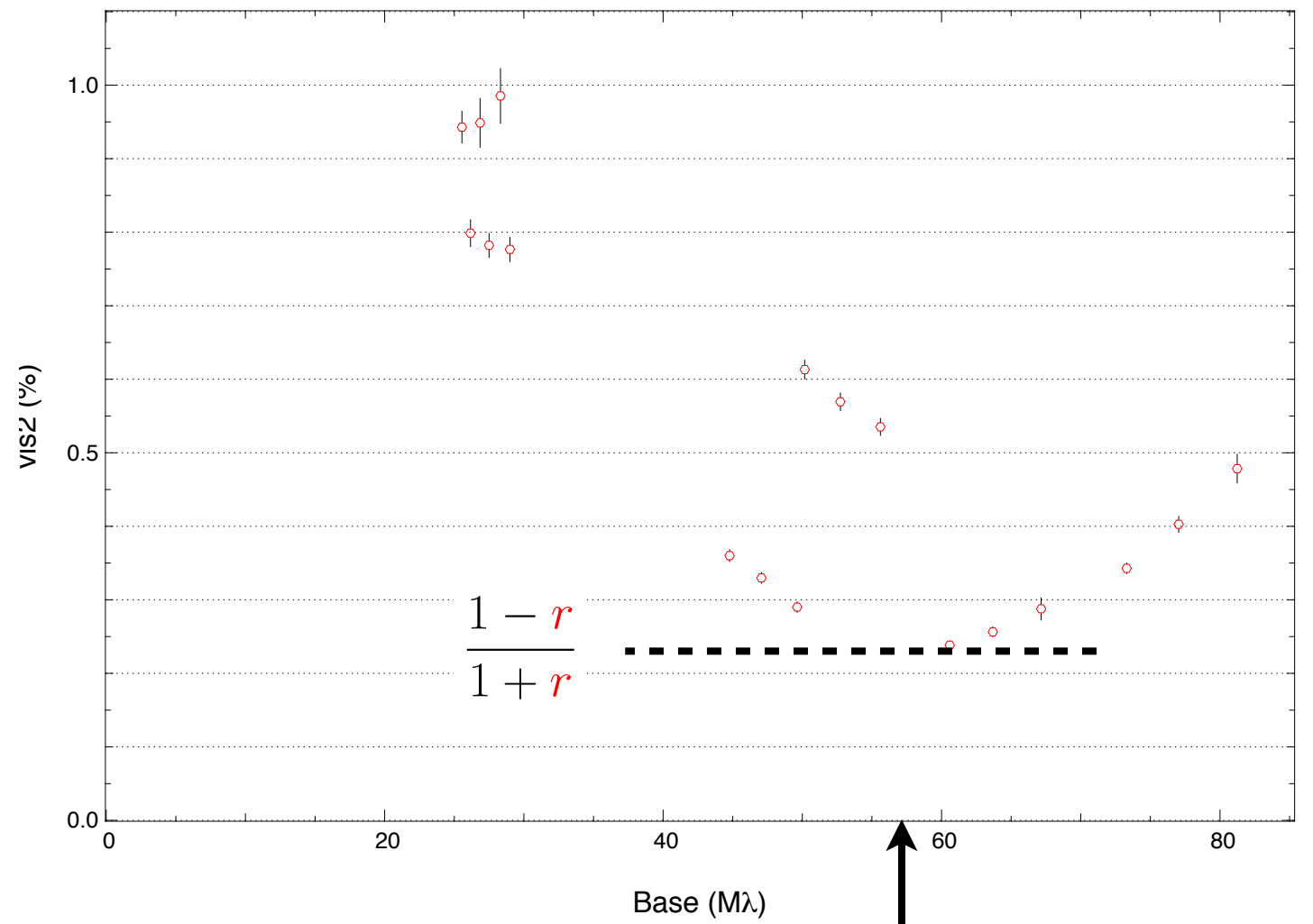
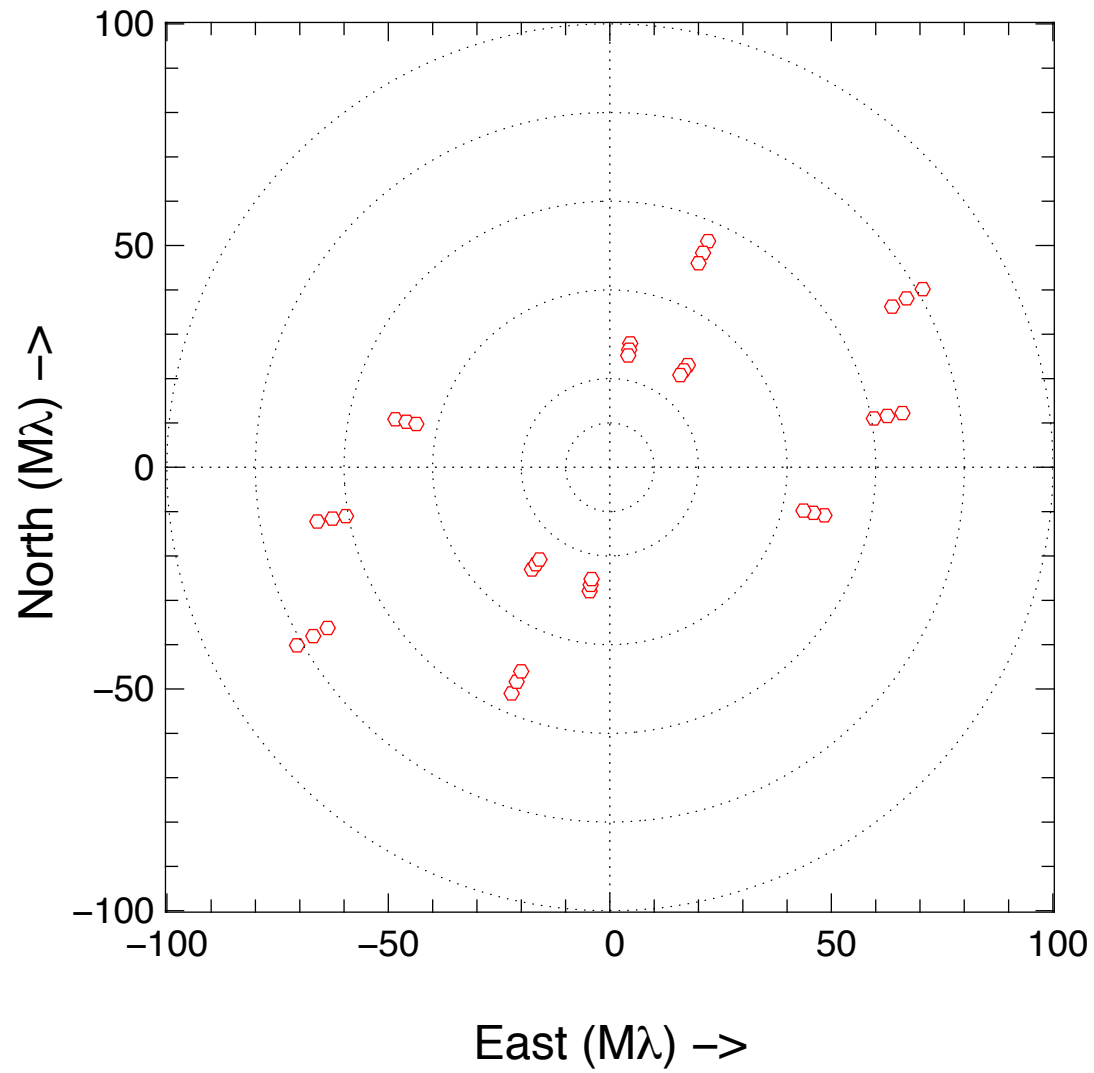
In the plane of the sky:

$$I = \delta(\vec{x}) + r \delta(\vec{x} - \vec{\rho})$$

Visibility = Fourier Transform:

$$V = \frac{1 + r e^{-2i\pi \frac{\vec{B}}{\lambda} \vec{\rho}}}{1 + r}$$

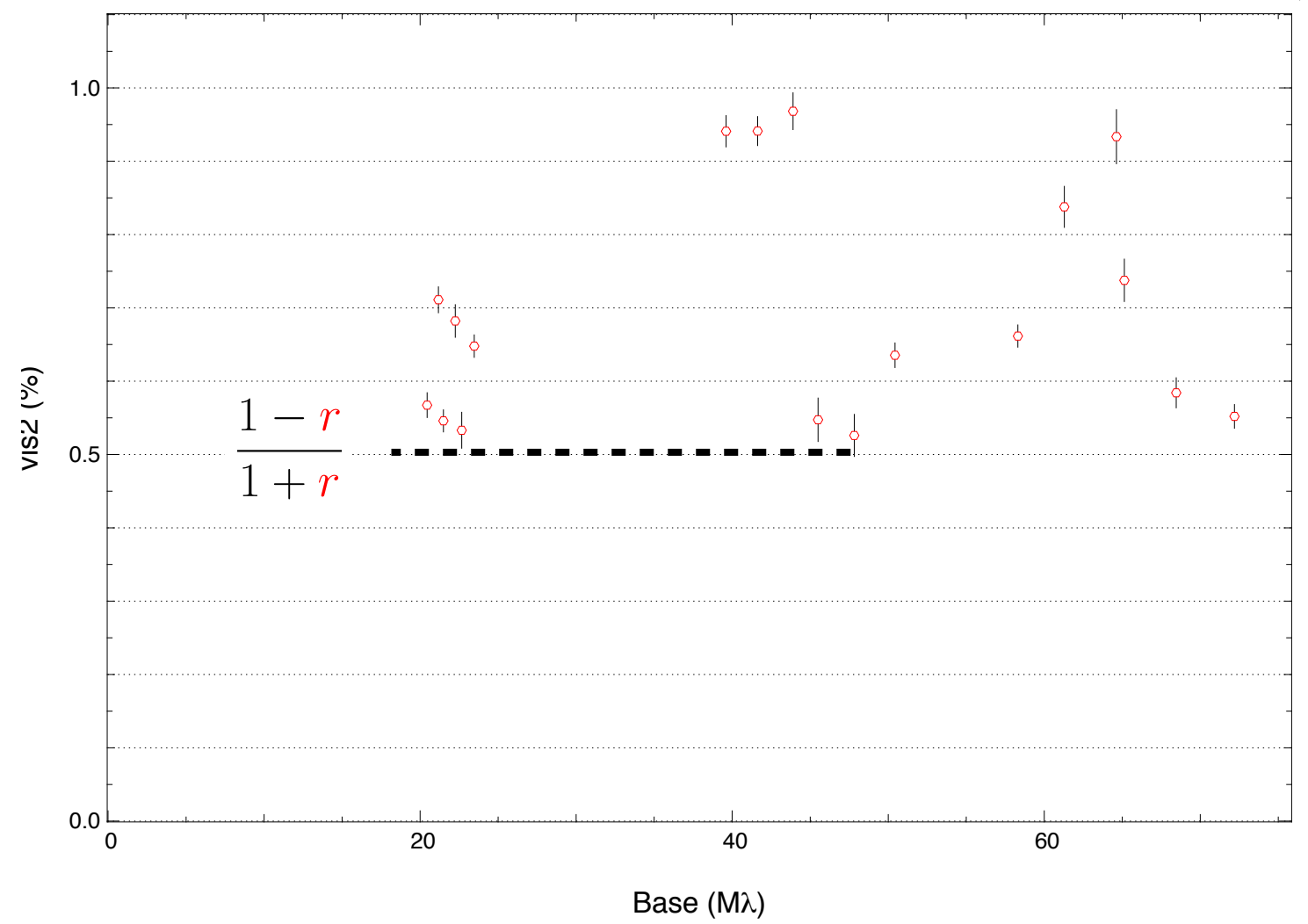
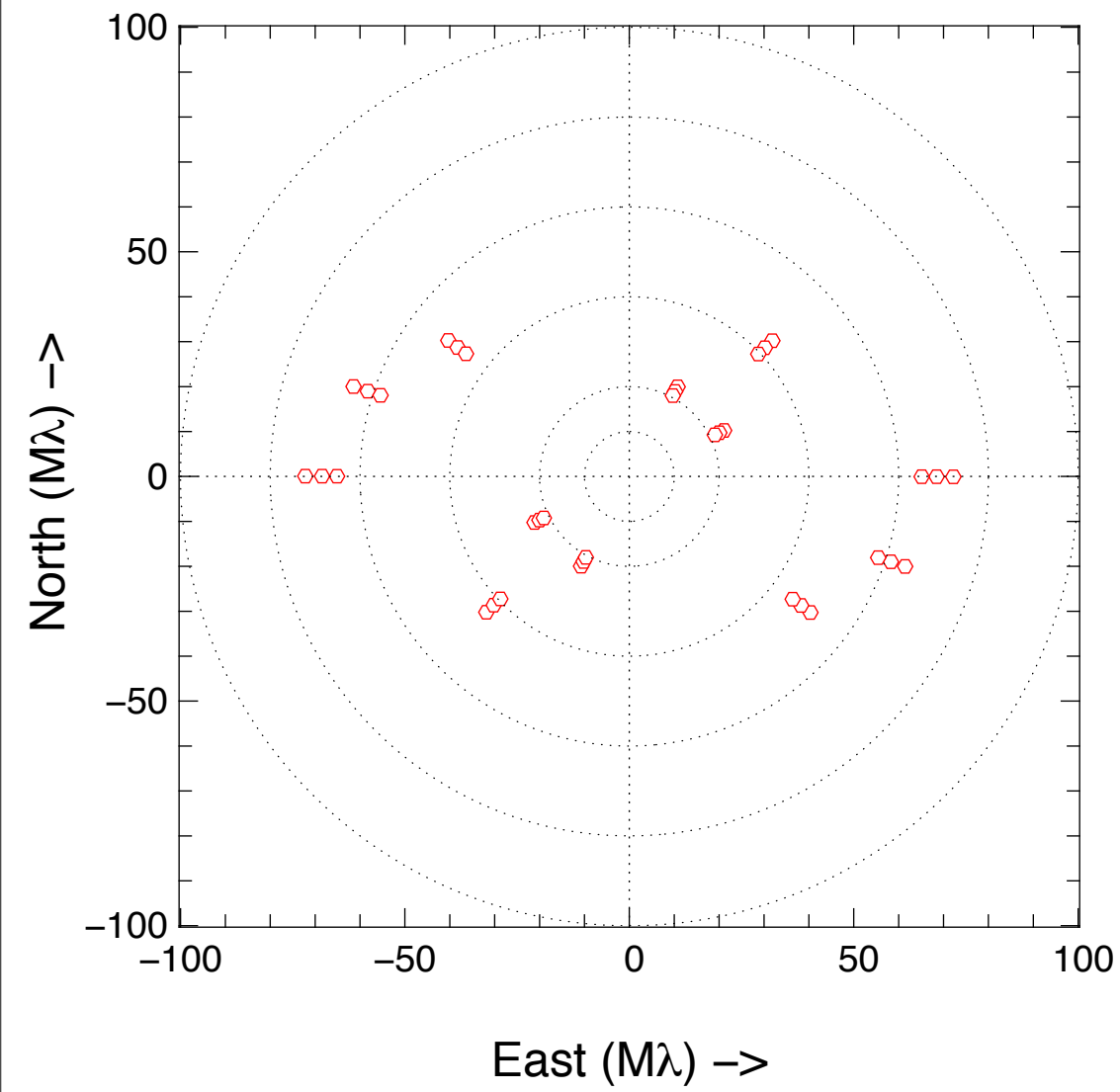
# HD 151003



$$V = \frac{1 + r e^{-2i\pi \frac{\vec{B}}{\lambda} \vec{\rho}}}{1 + r}$$

$$\frac{\vec{B}}{\lambda} \vec{\rho} = 0.5$$

# HD 97253



$$V = \frac{1 + r e^{-2i\pi \frac{\vec{B}}{\lambda} \vec{\rho}}}{1 + r}$$

# Some important aspect of the observation

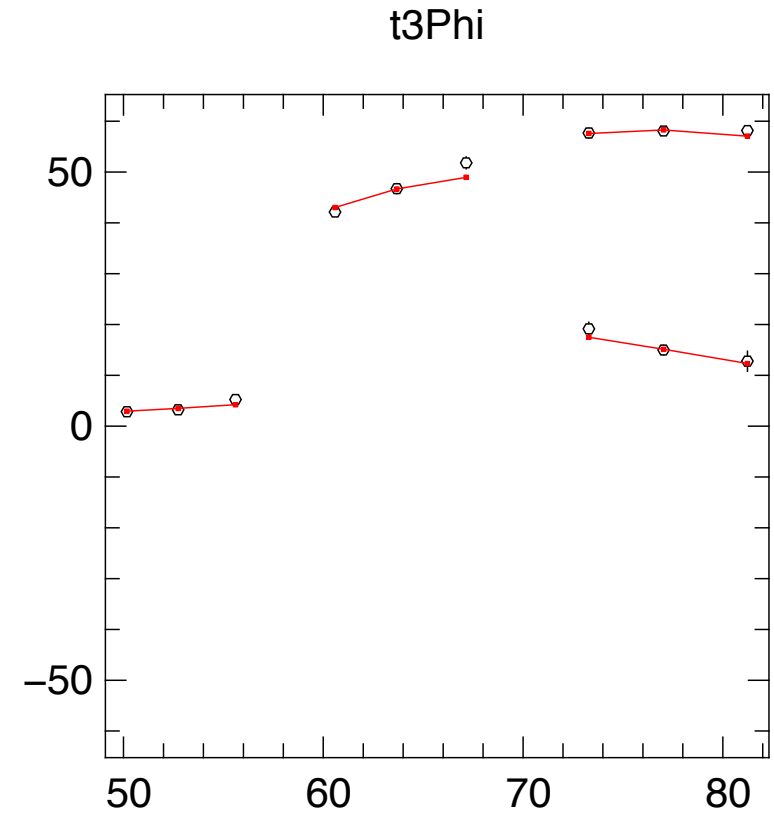
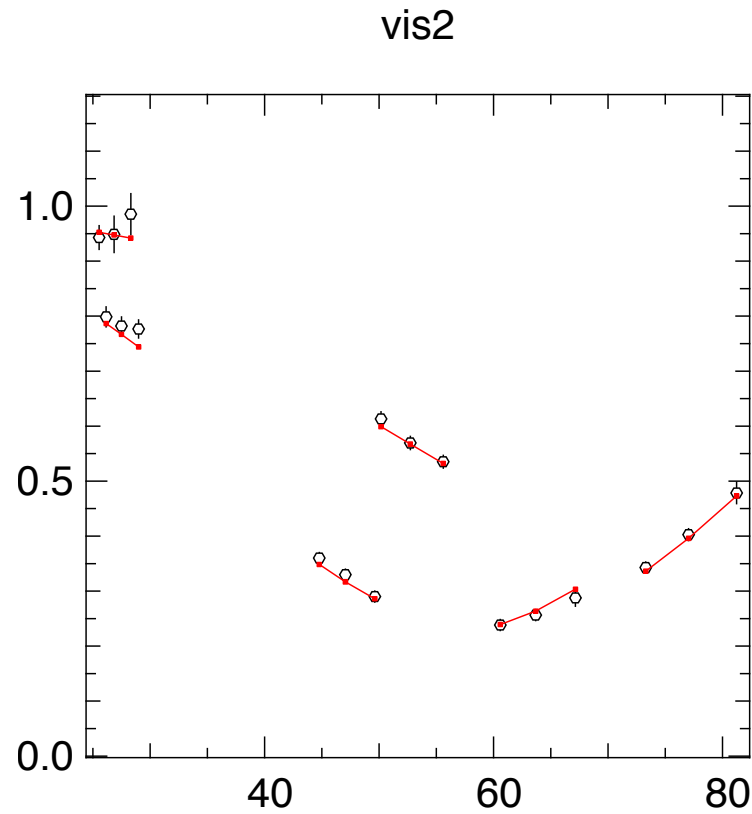
- Achievable spatial resolution
- Achievable dynamic
- Unambiguous field-of-view
- Smearing and outer-working-angle

# Spatial resolution: (I) easy

HD151003 (2012-06-11)

$$V = \frac{1 + r e^{-2i\pi \frac{\vec{B}}{\lambda} \vec{\rho}}}{1 + r}$$

$$\frac{\vec{B}_{max}}{\lambda} \vec{\rho} > 0.5$$



HD151003  
mjd=56089.153

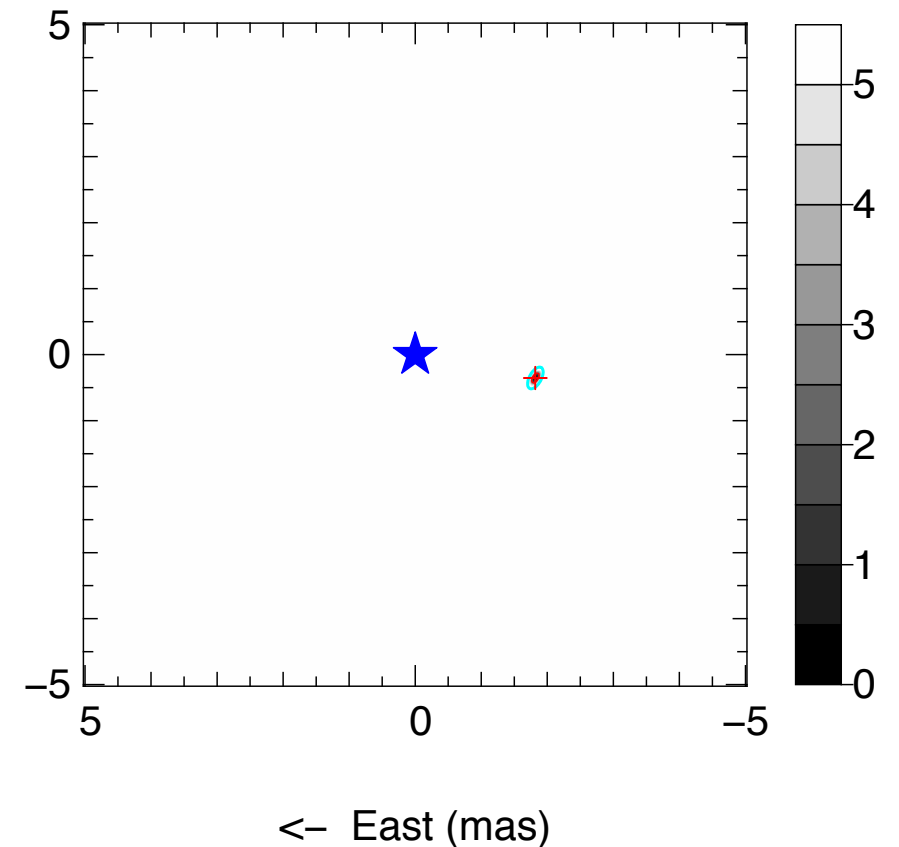
min(chi2)=1.1  
r=0.36\*

dE=-1.82mas\*  
dN=-0.35mas\*

$\rho=1.85\text{mas}$   
 $\theta=-101.0\text{deg}$   
 $\varepsilon=\{0.18\text{mas}, 0.09\text{mas}, 151\text{deg}\}$

2012-06-10\_SCI\_HD151003\_oiDataCalib

North (mas)  $\uparrow$



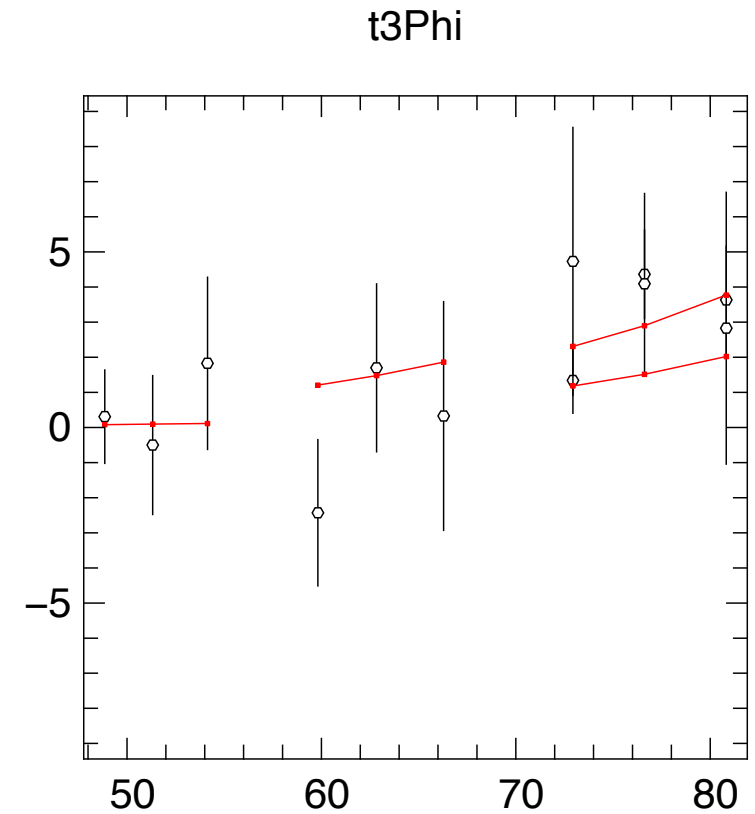
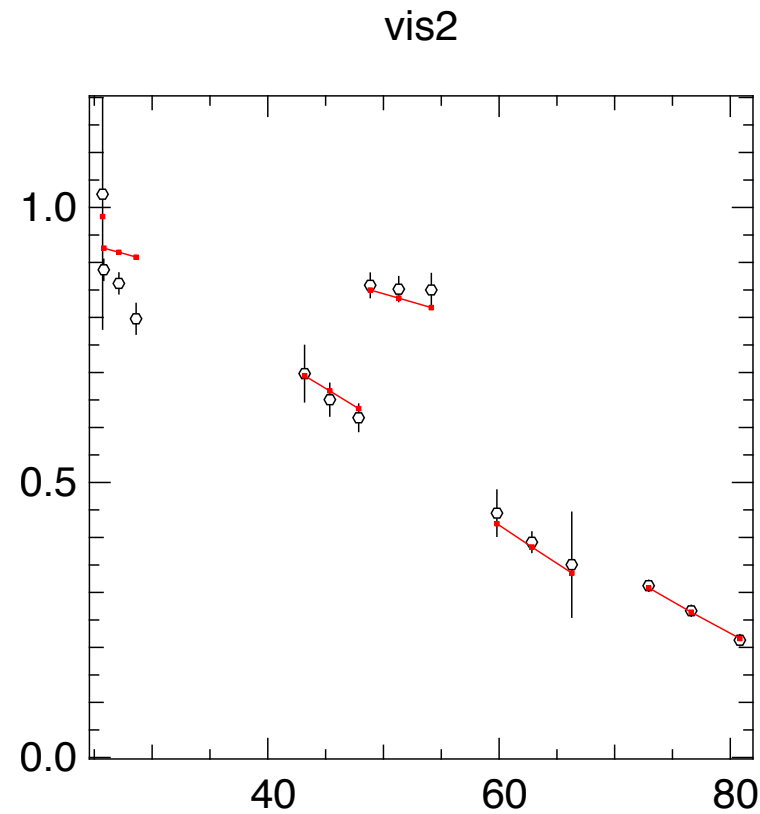
$\leftarrow$  East (mas)

# Spatial resolution: (2) getting closer

HD150135 (2012-06-10)

$$V = \frac{1 + r e^{-2i\pi \frac{\vec{B}}{\lambda} \vec{\rho}}}{1 + r}$$

$$\frac{\vec{B}_{max}}{\lambda} \vec{\rho} \approx 0.5$$



HD150135  
mjd=56088.128

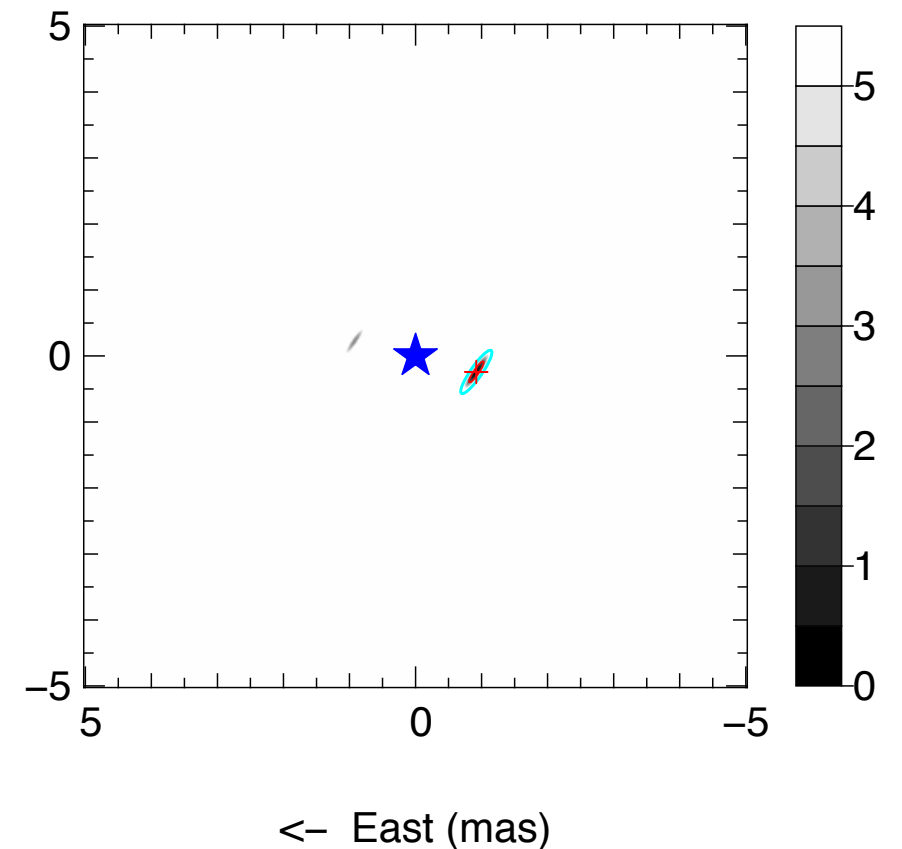
min(chi2)=1.5  
r=0.83\*

dE=-0.92mas\*  
dN=-0.24mas\*

$\rho=0.95\text{mas}$   
 $\theta=-104.7\text{deg}$   
 $\epsilon=\{0.39\text{mas}, 0.09\text{mas}, 145\text{deg}\}$

2012-06-09\_SCI\_HD150135\_oiDataCalib

North (mas)  $\uparrow$



$\leftarrow$  East (mas)

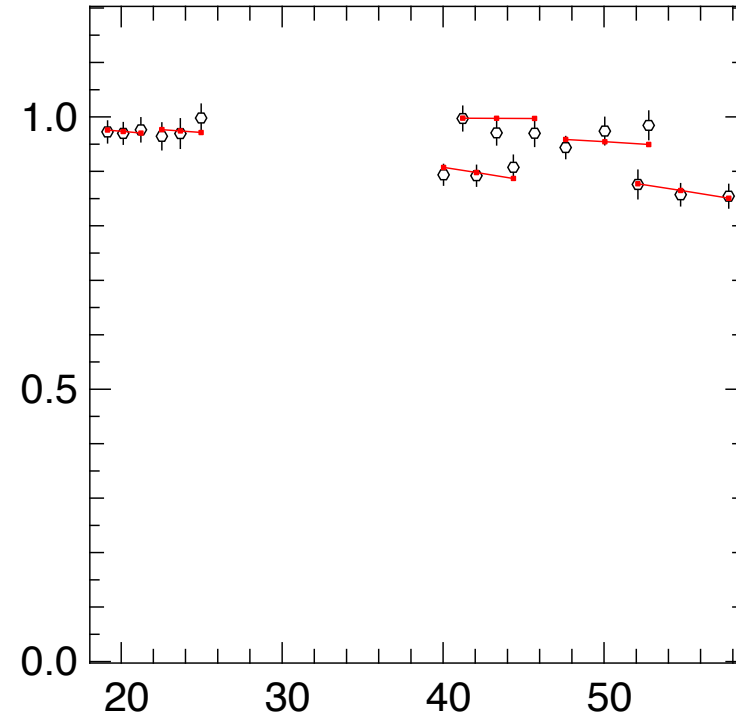
# Spatial resolution: (3) too compact

HD75759 (2012-06-10)

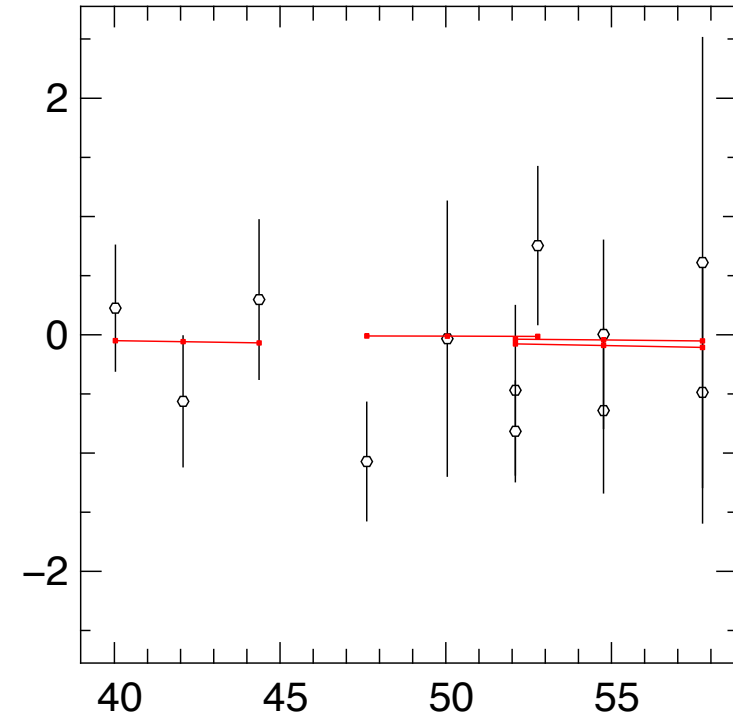
$$V = \frac{1 + r e^{-2i\pi \frac{\vec{B}}{\lambda} \vec{\rho}}}{1 + r}$$

$$\frac{\vec{B}_{max}}{\lambda} \vec{\rho} \ll 0.5$$

vis2



t3Phi



HD75759  
mjd=56088.985

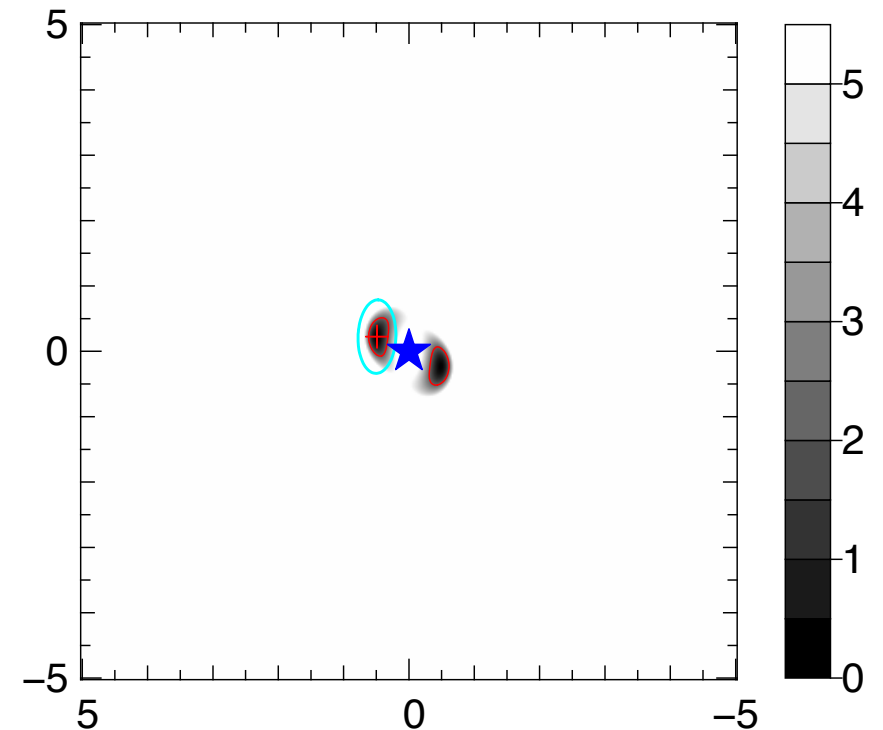
min(chi2)=0.7  
r=0.80 (fixed)

dE=0.49mas\*  
dN=0.23mas\*

$\rho=0.54\text{mas}$   
 $\theta=65.3\text{deg}$   
 $\epsilon=\{0.56\text{mas}, 0.29\text{mas}, 178\text{deg}\}$

2012-06-10\_SCI\_HD75759\_oiDataCalib

North (mas) →



← East (mas)

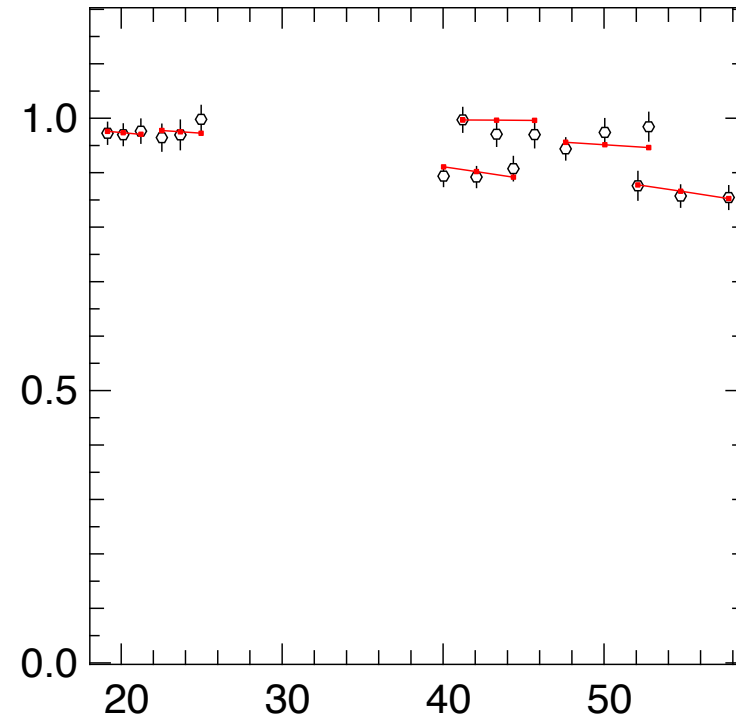
# Spatial resolution: (3) too compact

HD75759 (2012-06-10)

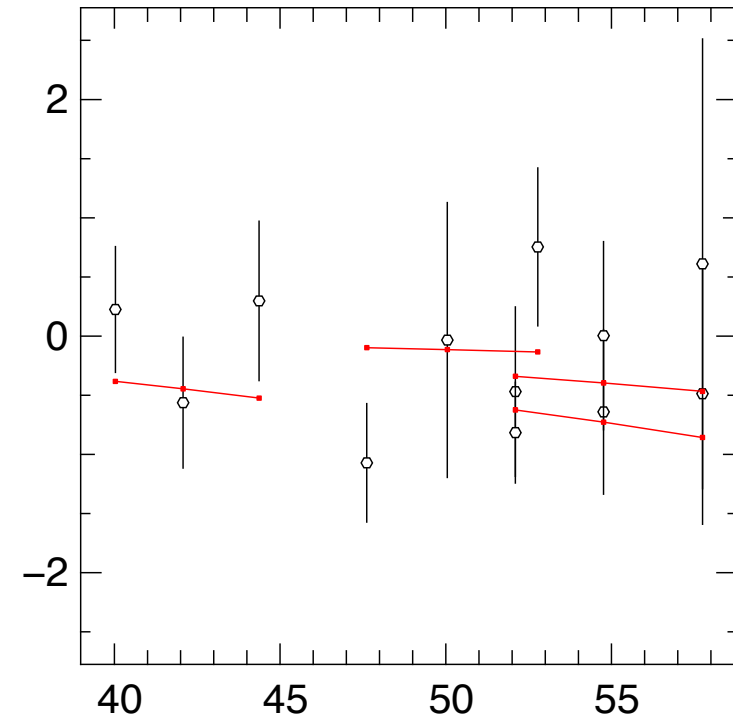
$$V = \frac{1 + r e^{-2i\pi \frac{\vec{B}}{\lambda} \vec{\rho}}}{1 + r}$$

$$\frac{\vec{B}_{max}}{\lambda} \vec{\rho} \ll 0.5$$

vis2



t3Phi



HD75759  
mjd=56088.985

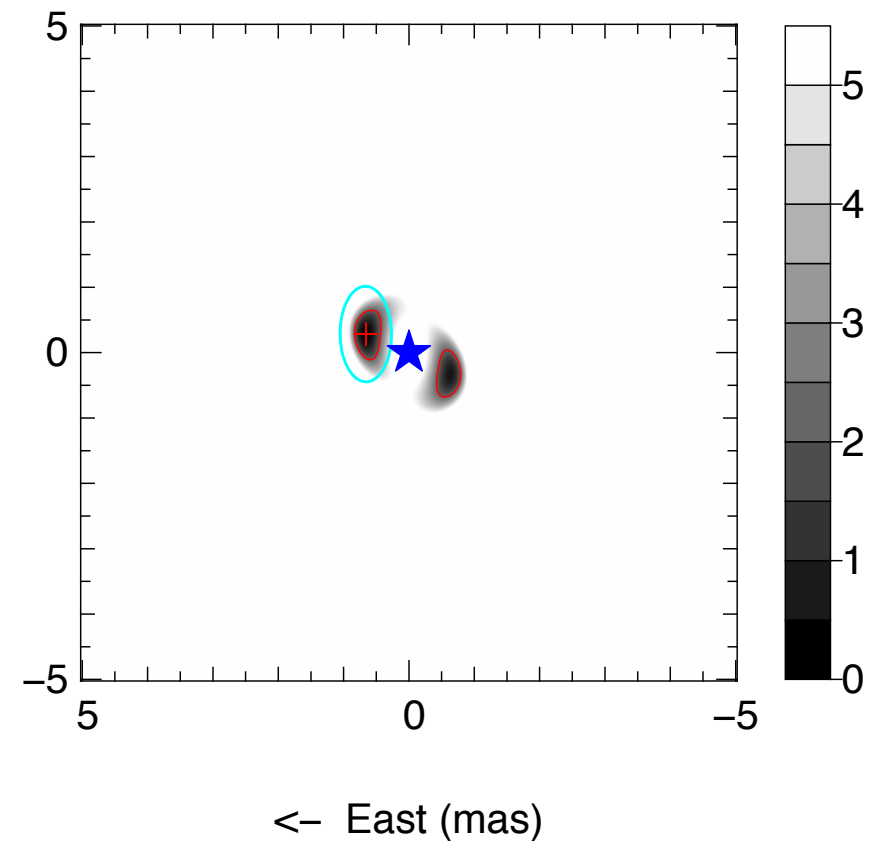
min(chi2)=0.7  
r=0.20 (fixed)

dE=0.66mas\*  
dN=0.28mas\*

$\rho=0.72\text{mas}$   
 $\theta=66.7\text{deg}$   
 $\epsilon=\{0.73\text{mas}, 0.39\text{mas}, 1\text{deg}\}$

2012-06-10\_SCI\_HD75759\_oiDataCalib

North (mas)  $\uparrow$



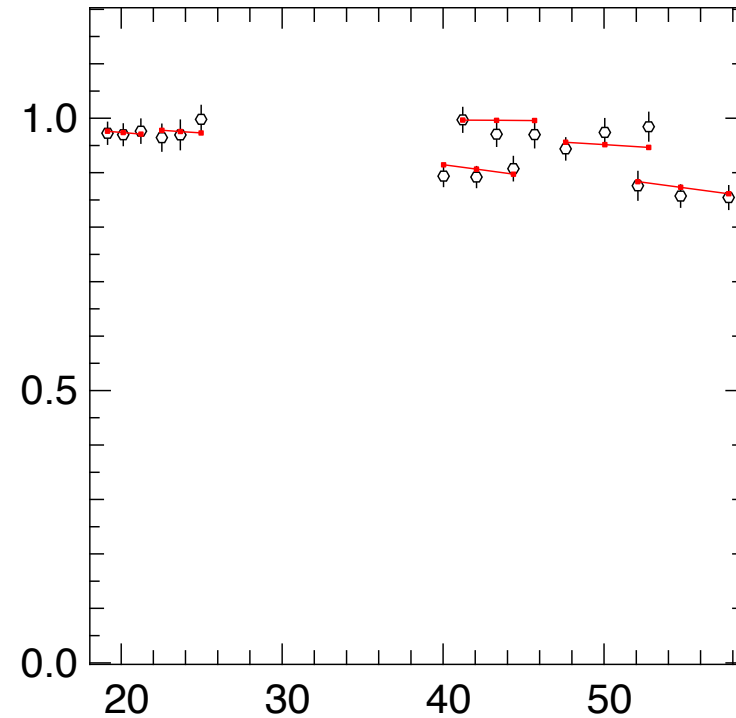
# Spatial resolution: (3) too compact

HD75759 (2012-06-10)

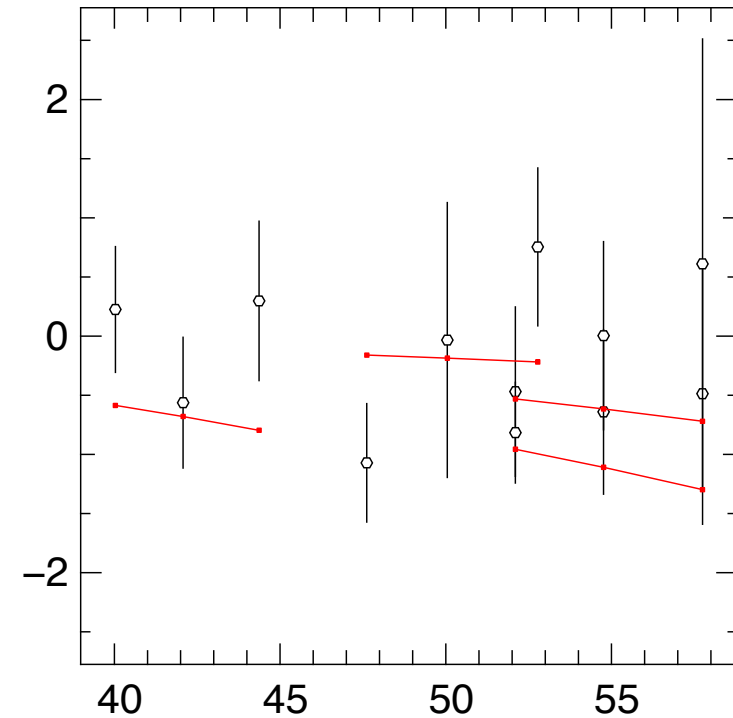
$$V = \frac{1 + r e^{-2i\pi \frac{\vec{B}}{\lambda} \vec{\rho}}}{1 + r}$$

$$\frac{\vec{B}_{max}}{\lambda} \vec{\rho} \ll 0.5$$

vis2



t3Phi



HD75759  
mjd=56088.985

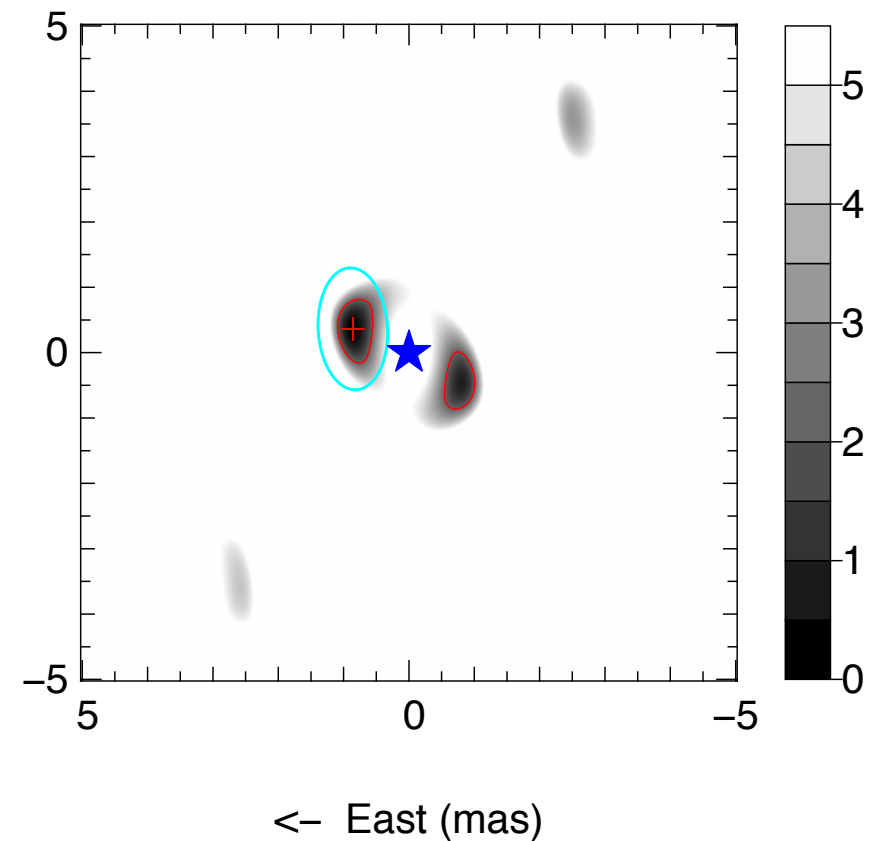
min(chi2)=0.8  
r=0.10 (fixed)

dE=0.86mas\*  
dN=0.36mas\*

$\rho=0.93\text{mas}$   
 $\theta=67.0\text{deg}$   
 $\epsilon=\{0.93\text{mas}, 0.53\text{mas}, 3\text{deg}\}$

2012-06-10\_SCI\_HD75759\_oiDataCalib

North (mas)  $\uparrow$



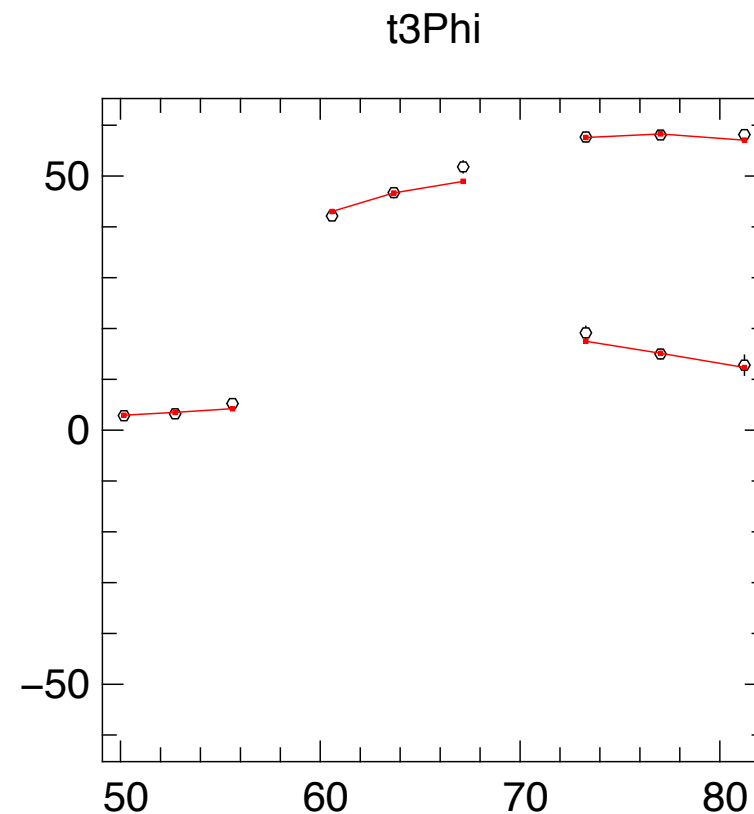
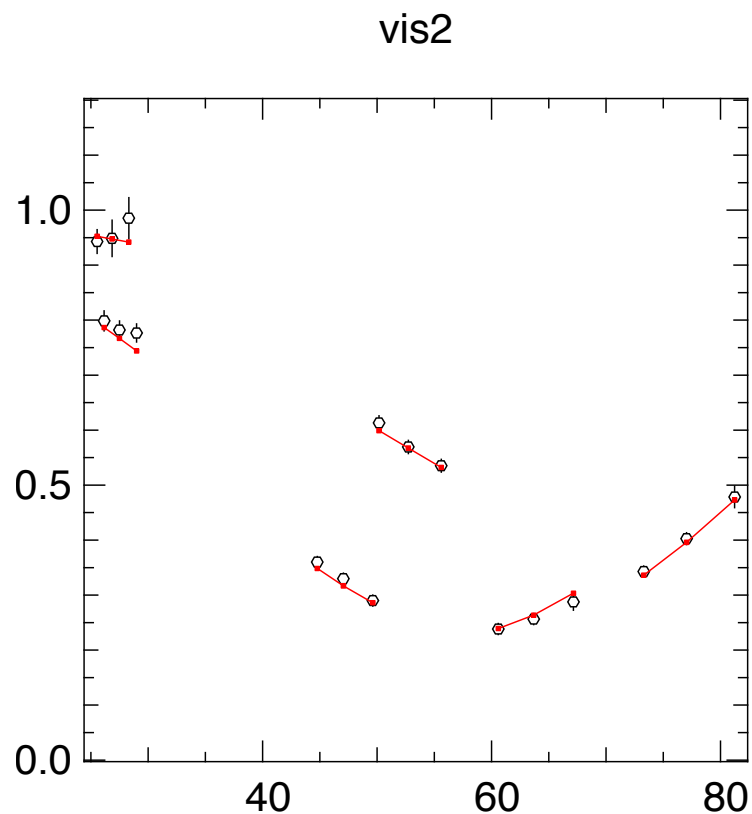
$\leftarrow$  East (mas)

# Spatial resolution: (4) back to resolved

HD151003 (2012-06-11)

$$V = \frac{1 + r e^{-2i\pi \frac{\vec{B}}{\lambda} \vec{\rho}}}{1 + r}$$

$$\frac{\vec{B}_{max}}{\lambda} \vec{\rho} > 0.5$$



HD151003  
mjd=56089.153

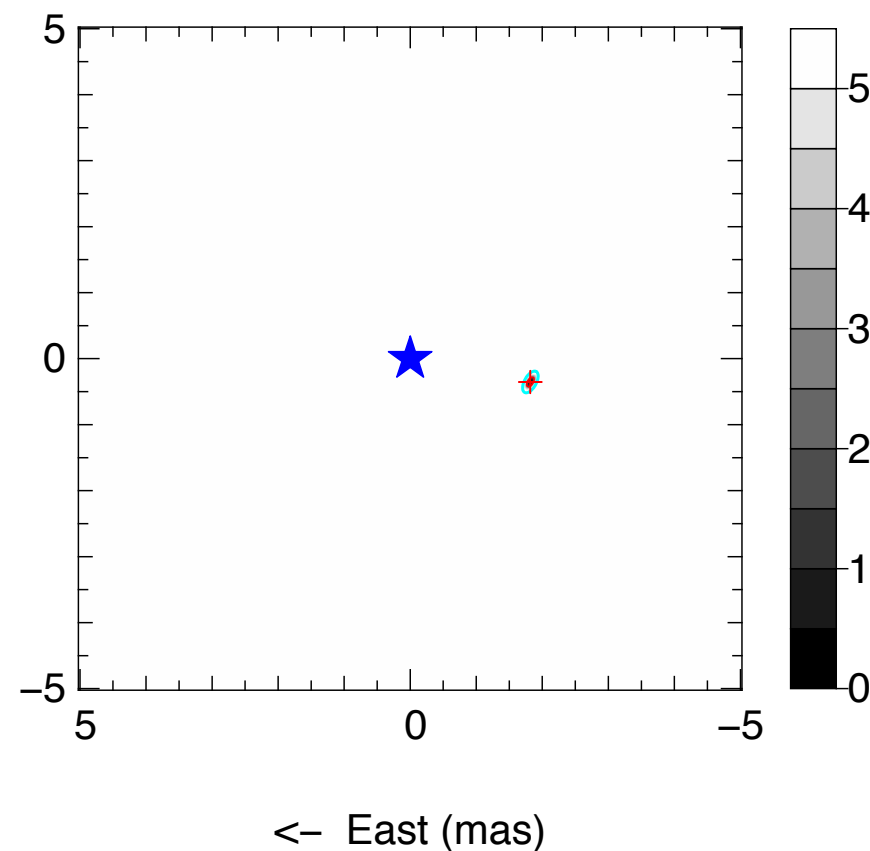
min(chi2)=1.1  
r=0.36\*

dE=-1.82mas\*  
dN=-0.35mas\*

$\rho=1.85\text{mas}$   
 $\theta=-101.0\text{deg}$   
 $\varepsilon=\{0.18\text{mas}, 0.09\text{mas}, 151\text{deg}\}$

2012-06-10\_SCI\_HD151003\_oiDataCalib

North (mas)  $\uparrow$

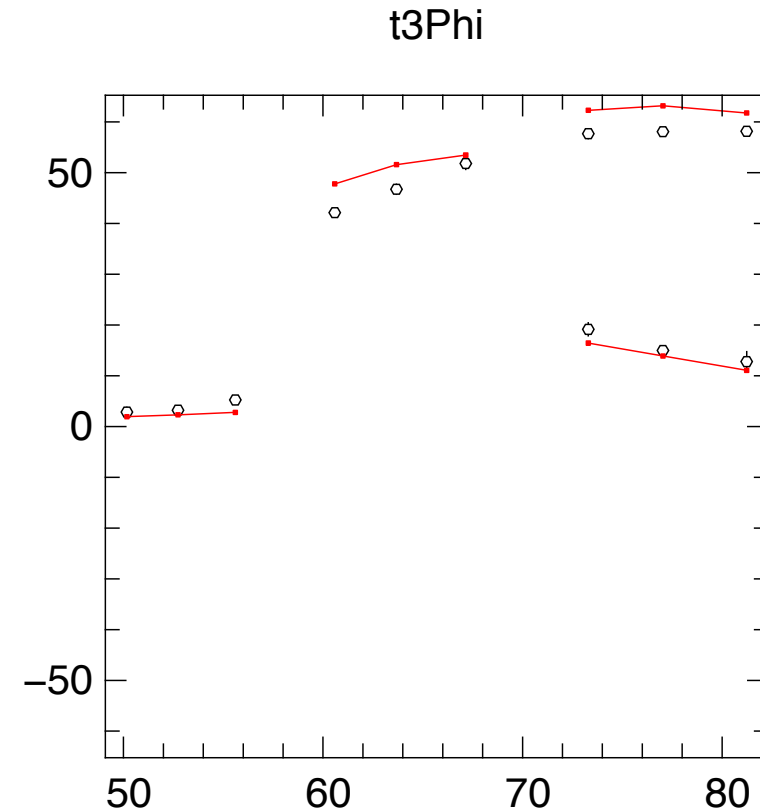
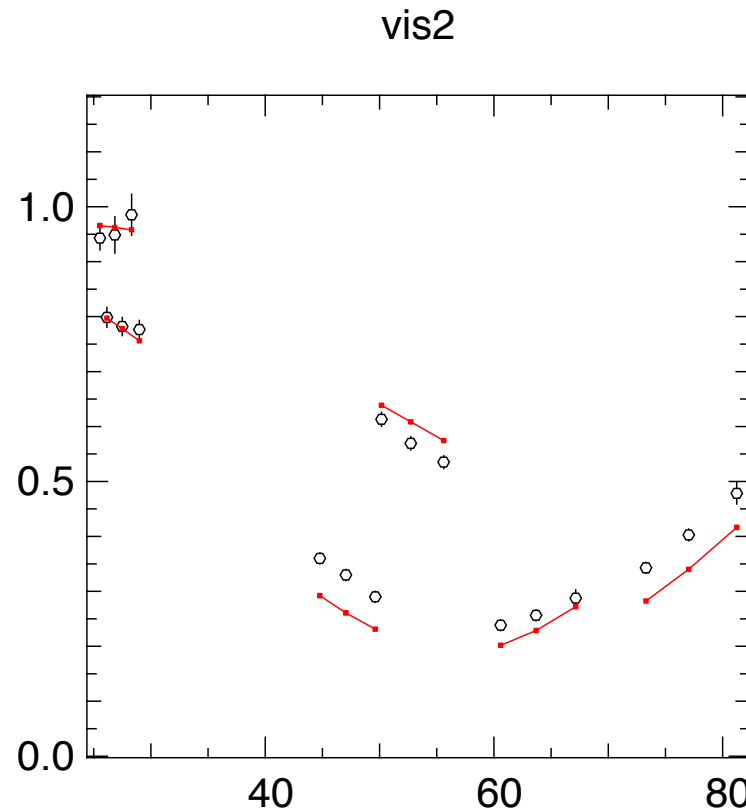


# Spatial resolution: (4) back to resolved

HD151003 (2012-06-11)

$$V = \frac{1 + r e^{-2i\pi \frac{\vec{B}}{\lambda} \vec{\rho}}}{1 + r}$$

$$\frac{\vec{B}_{max}}{\lambda} \vec{\rho} > 0.5$$



HD151003  
mjd=56089.153

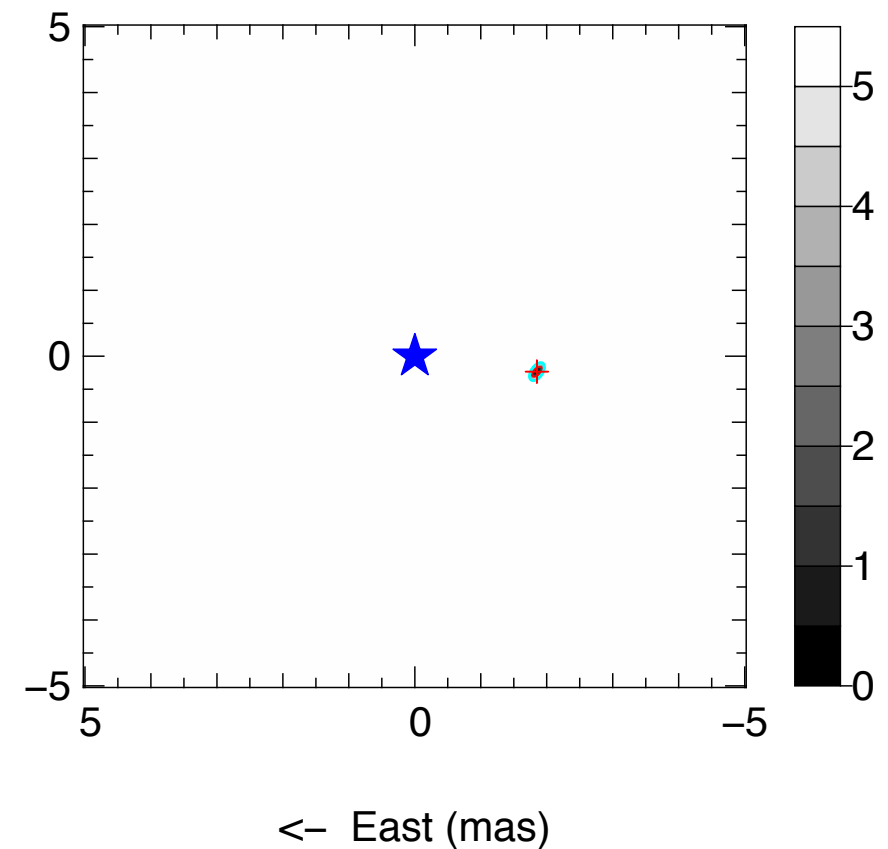
min(chi2)=16.9  
r=0.40

dE=-1.85mas\*  
dN=-0.23mas\*

$\rho=1.87\text{mas}$   
 $\theta=-97.2\text{deg}$   
 $\varepsilon=\{0.15\text{mas}, 0.09\text{mas}, 145\text{deg}\}$

2012-06-10\_SCI\_HD151003\_oiDataCalib

North (mas)  $\uparrow$

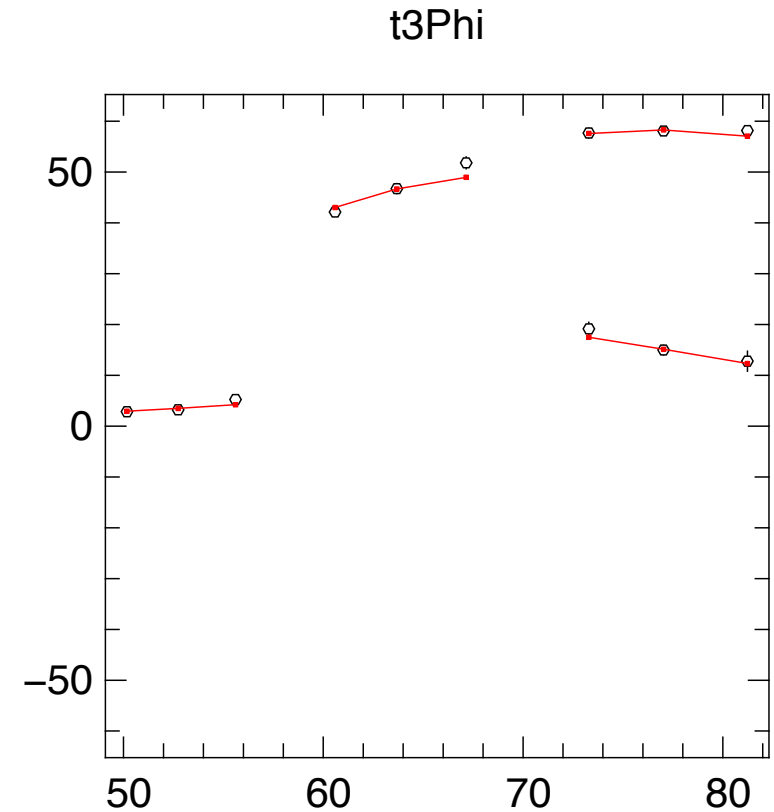
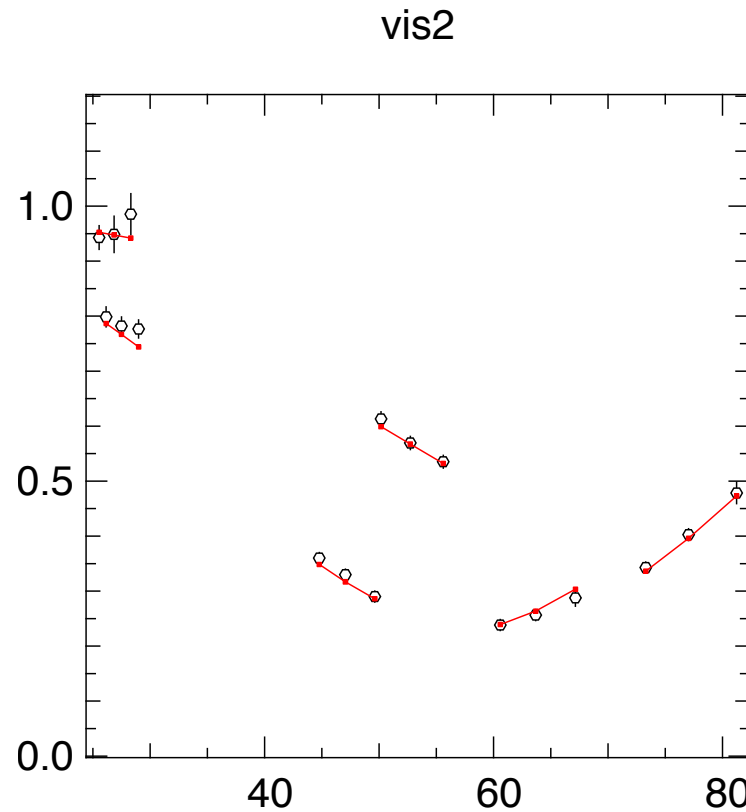


# Achievable dynamic: (I) a 30% contrast detection

HD151003 (2012-06-11)

$$V = \frac{1 + r e^{-2i\pi \frac{\vec{B}}{\lambda} \vec{\rho}}}{1 + r}$$

$$\frac{1 - r}{1 + r} > \sigma_V$$



HD151003  
mjd=56089.153

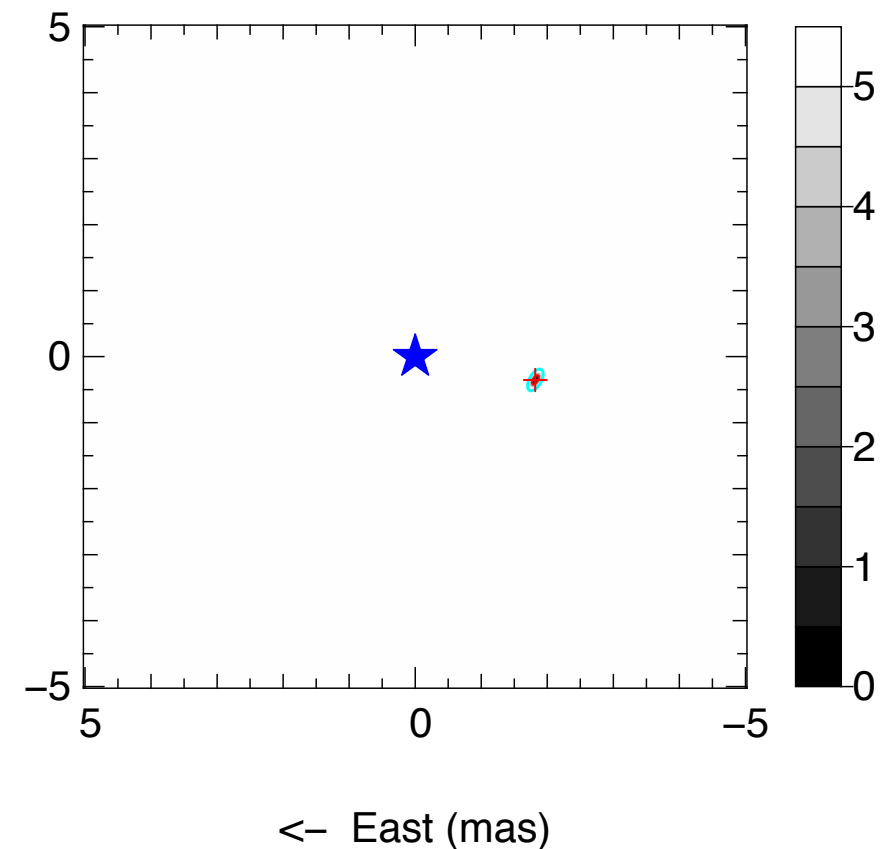
min(chi2)=1.1  
r=0.36\*

dE=-1.82mas\*  
dN=-0.35mas\*

$\rho=1.85\text{mas}$   
 $\theta=-101.0\text{deg}$   
 $\varepsilon=\{0.18\text{mas}, 0.09\text{mas}, 151\text{deg}\}$

2012-06-10\_SCI\_HD151003\_oiDataCalib

North (mas)  $\uparrow$



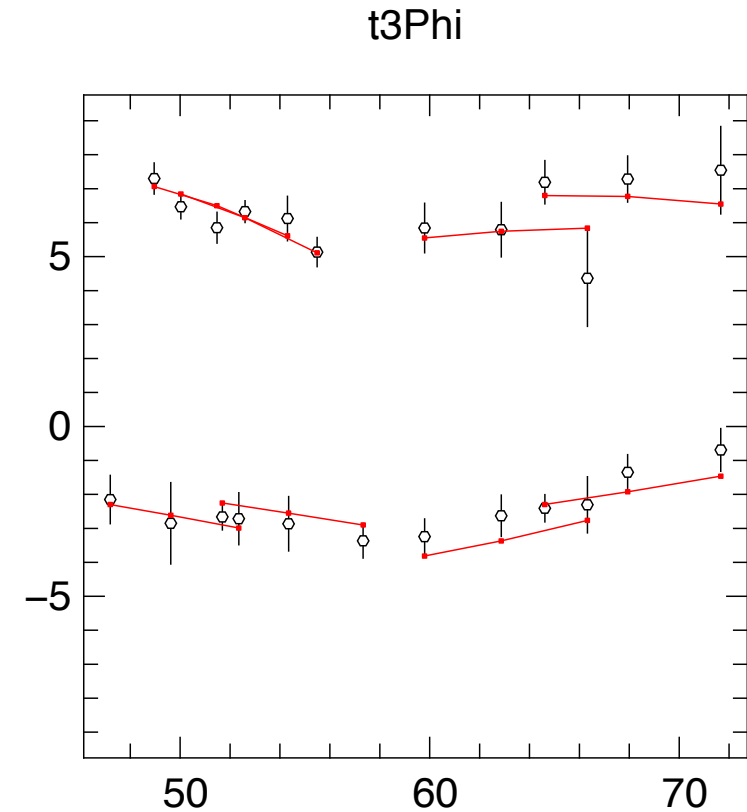
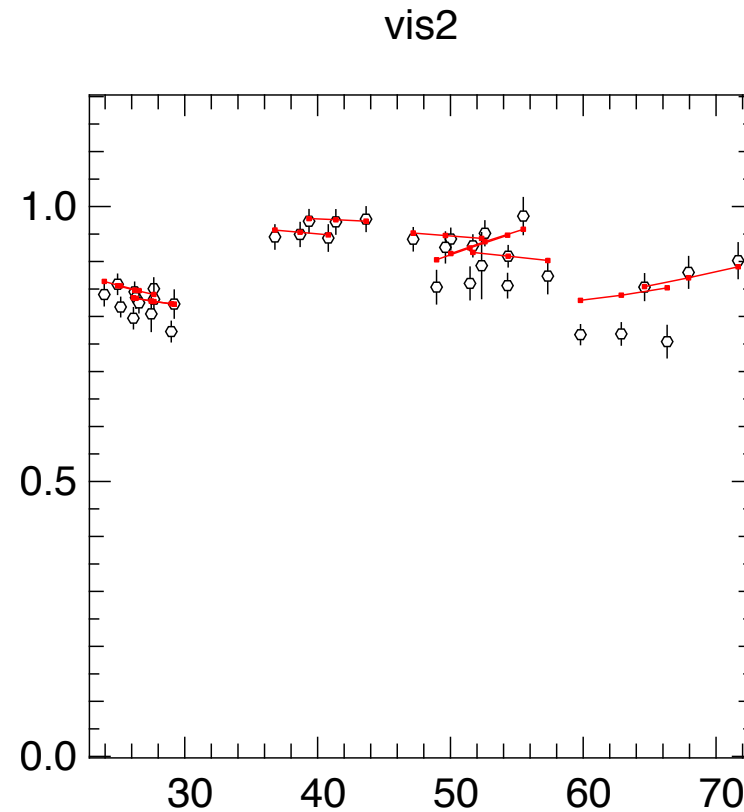
$\leftarrow$  East (mas)

# Achievable dynamic: (I) a 5% contrast detection

15\_SGR (2012-09-18)

$$V = \frac{1 + r e^{-2i\pi \frac{\vec{B}}{\lambda} \vec{\rho}}}{1 + r}$$

$$\frac{1 - r}{1 + r} > \sigma_V$$



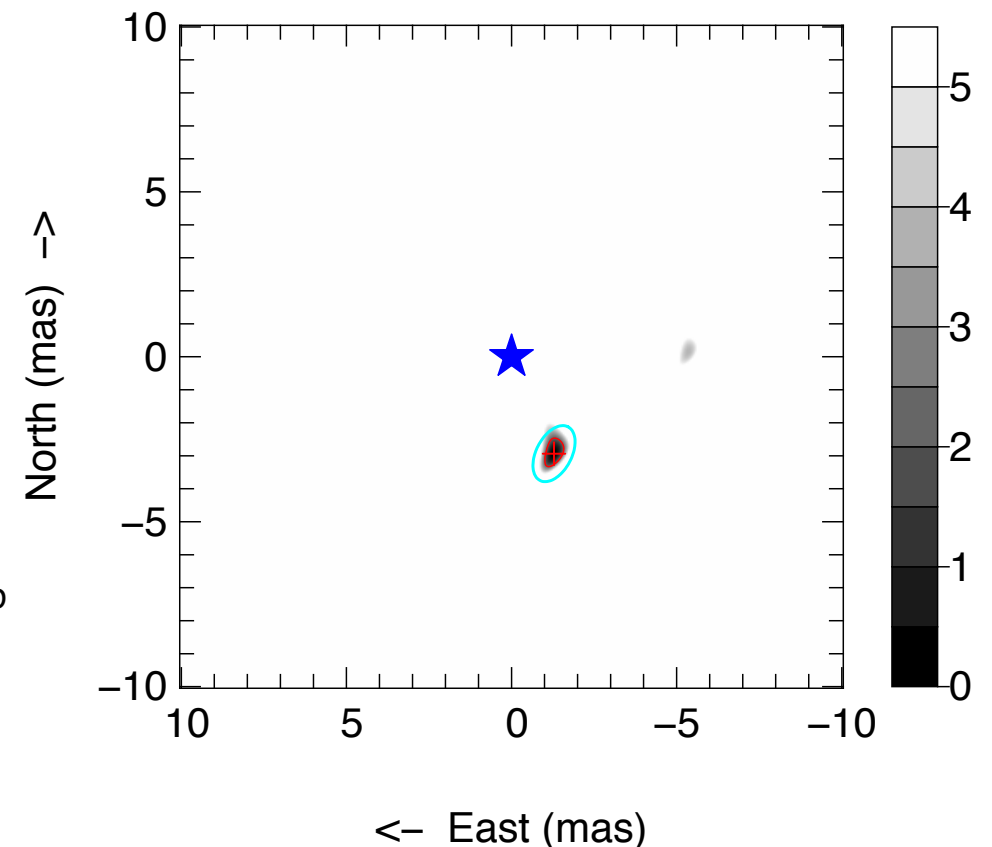
15\_SGR  
mjd=56188.070

min(chi2)=1.7  
r=0.05

dE=-1.29mas\*  
dN=-2.94mas\*

$\rho=3.20\text{mas}$   
 $\theta=-156.3\text{deg}$   
 $\varepsilon=\{0.92\text{mas}, 0.54\text{mas}, 152\text{deg}\}$

2012-09-17\_SCI\_15\_SGR\_oiDataCalib



# Achievable dynamic: (2) a 5% contrast non-detection

PLASKETT (2013-01-24)

$$V = \frac{1 + r e^{-2i\pi \frac{\vec{B}}{\lambda} \vec{\rho}}}{1 + r}$$

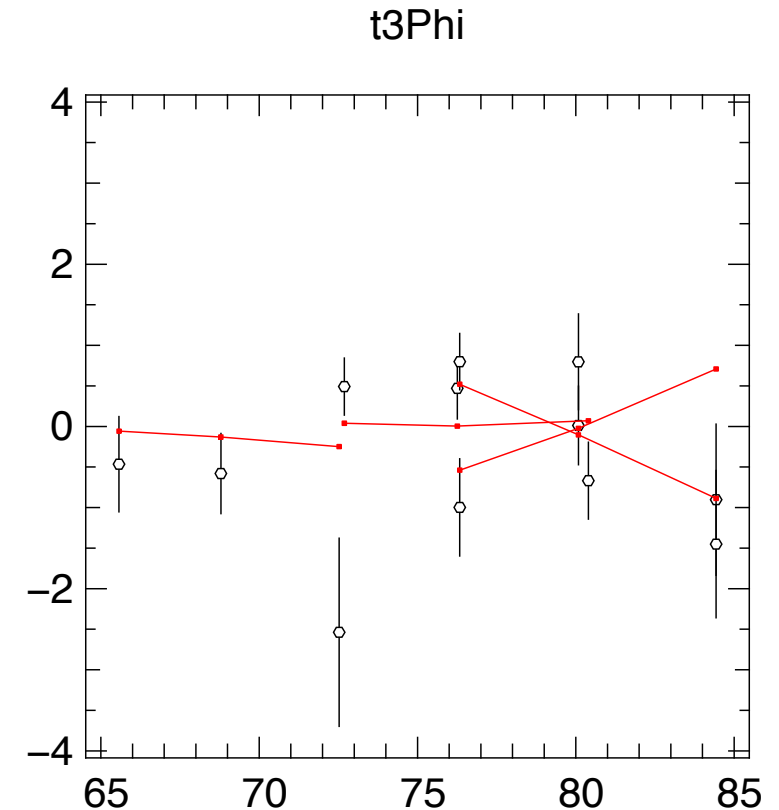
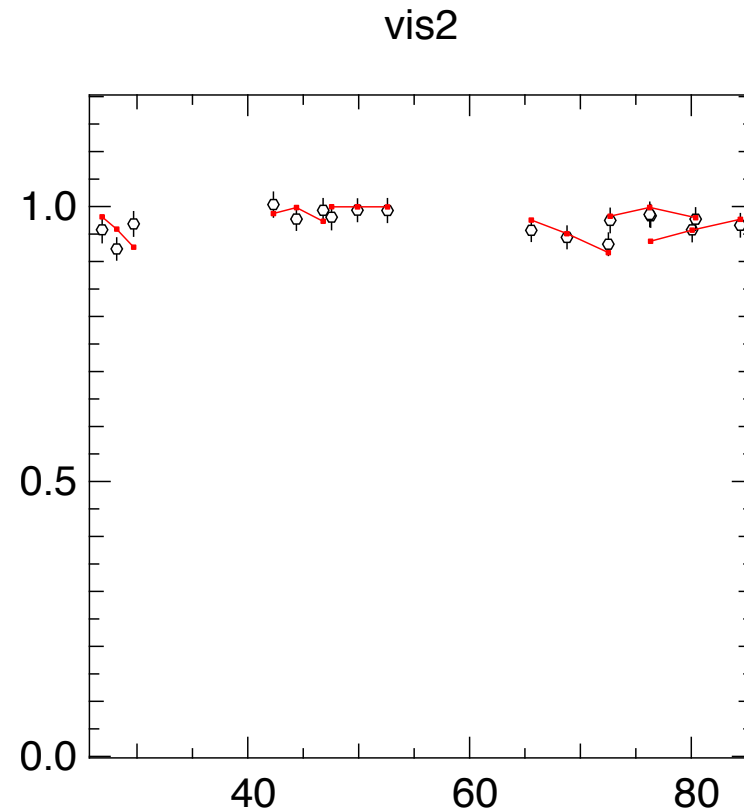
If you want to have good chance to detect  $r$ , you need a precision:

$$\frac{1 - r}{1 + r} > \sigma_V$$

If you have this precision, you cannot fully discard a binary of ratio  $r \Rightarrow$  “blind spots”.

If you have plenty of baselines  $\Rightarrow$  no more “blind spots”, the achievable dynamics  $r$  is given by:

$$\frac{1 - r}{1 + r} \approx \sigma_V$$



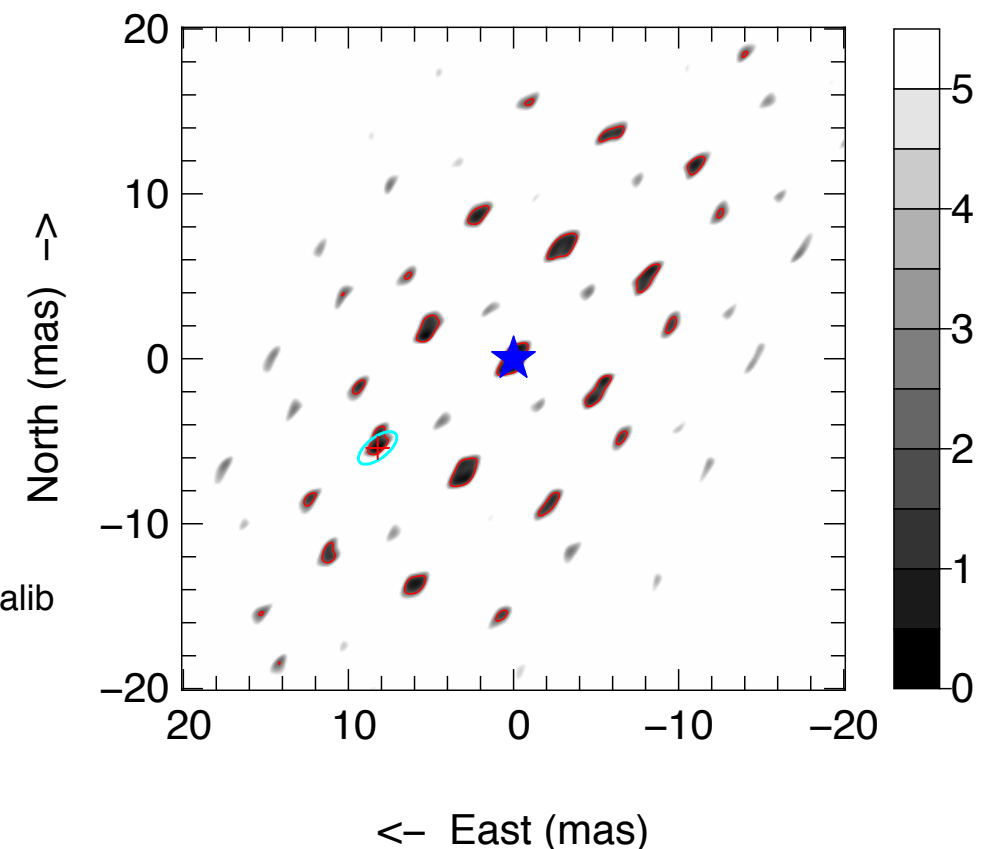
PLASKETT  
mjd=56316.161

min(chi2)=1.3  
r=0.05

dE=8.23mas\*  
dN=-5.40mas\*

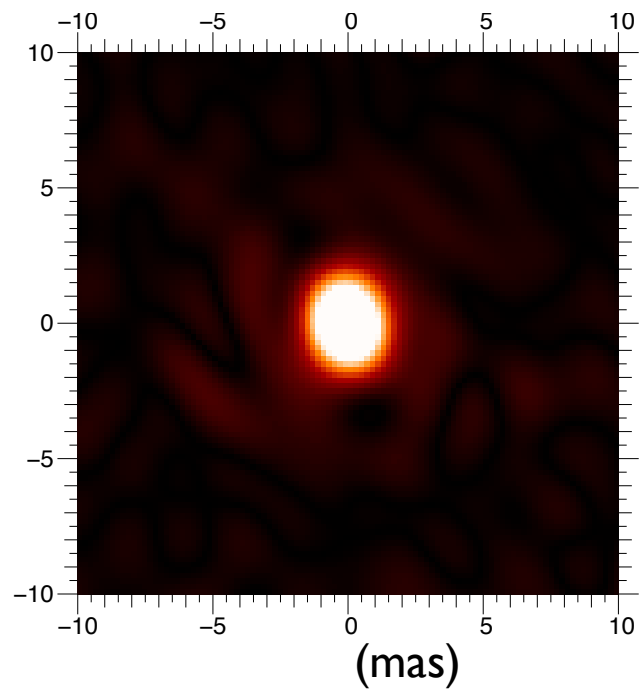
$\rho=9.85\text{mas}$   
 $\theta=123.3\text{deg}$   
 $\varepsilon=\{1.38\text{mas}, 0.64\text{mas}, 128\text{deg}\}$

2013-01-23\_SCI\_PLASKETT\_oiDataCalib

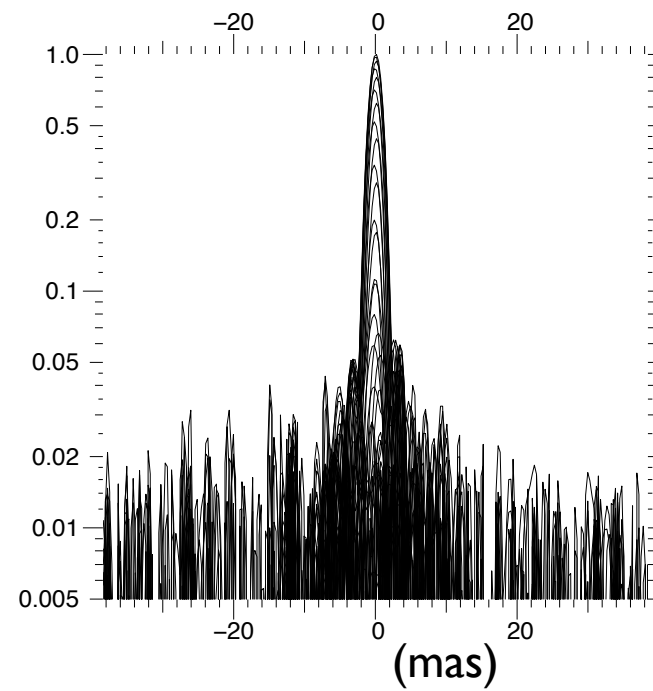


# Achievable dynamic: (3) eta Carinae

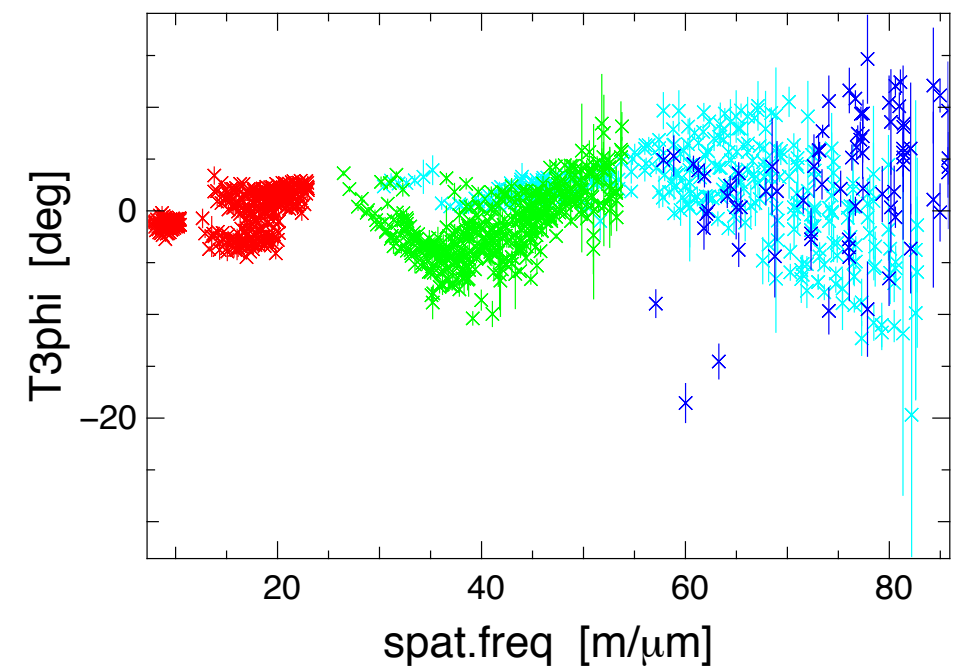
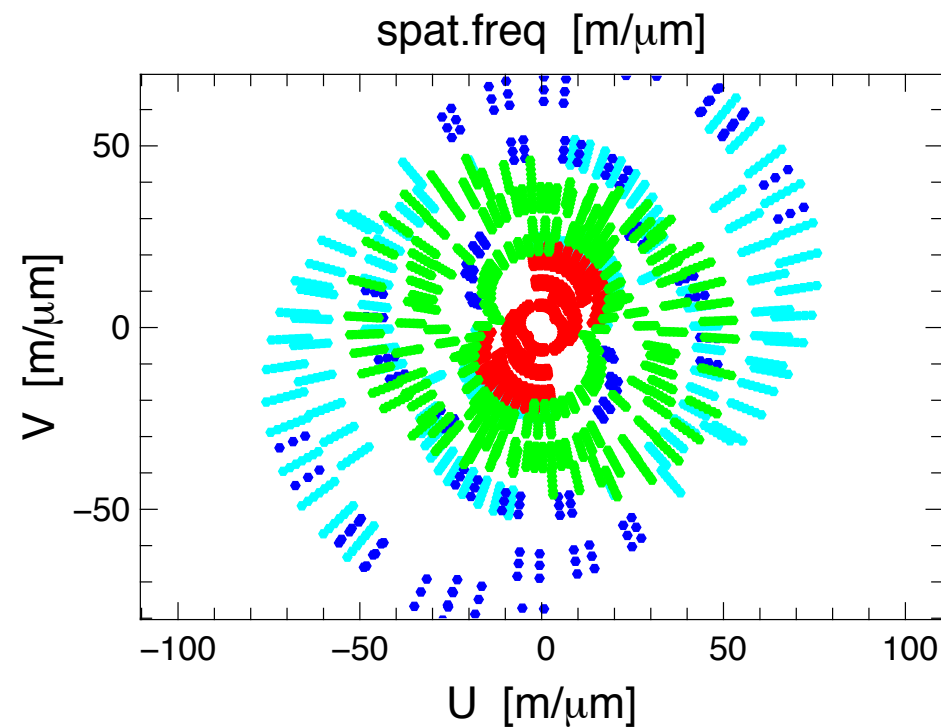
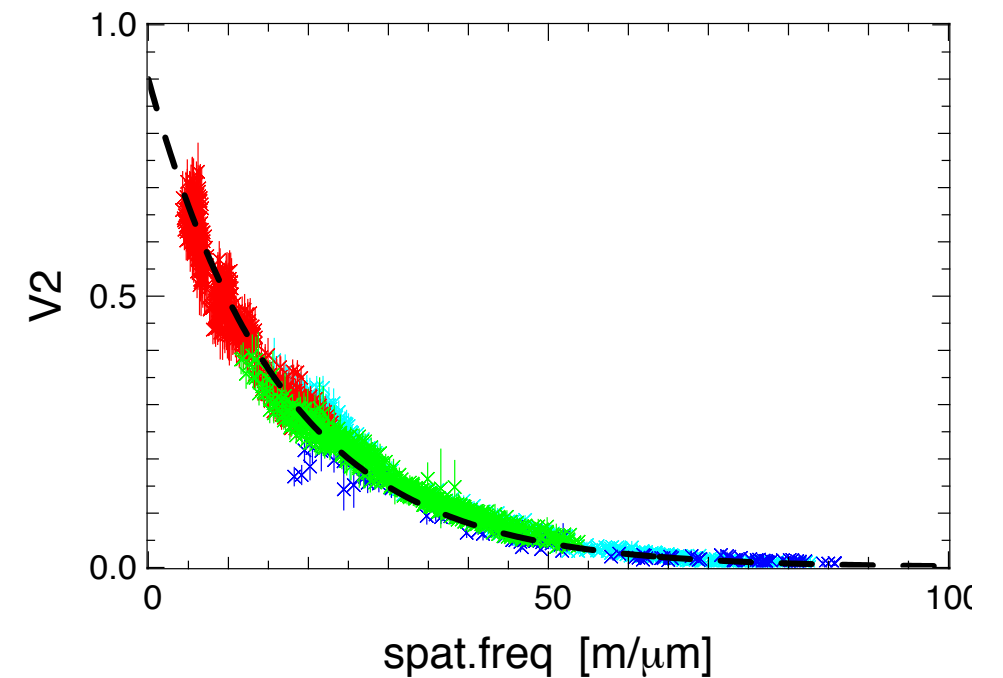
Image reconstruction



Cuts through the image



Observations



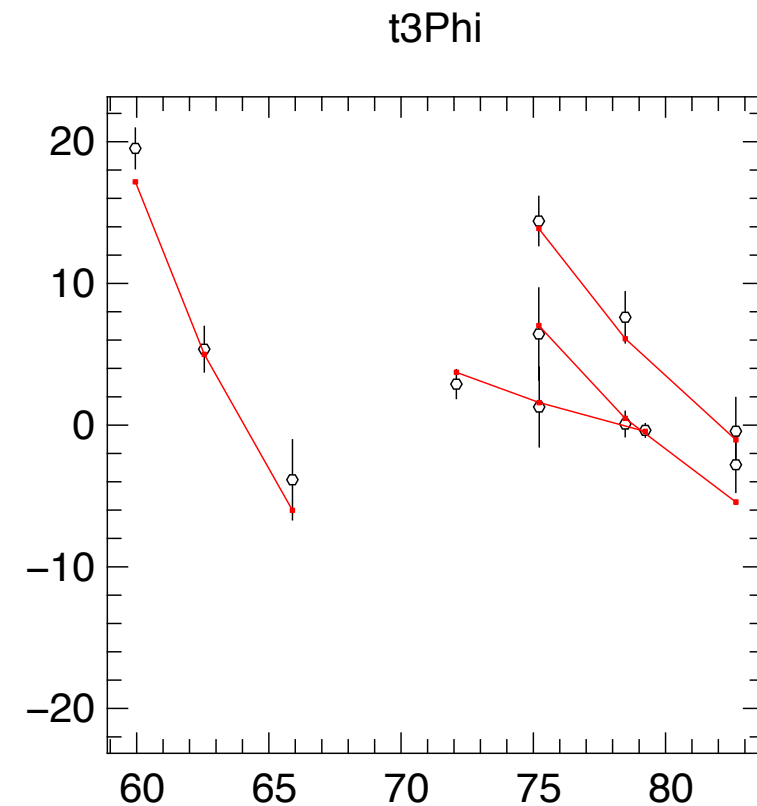
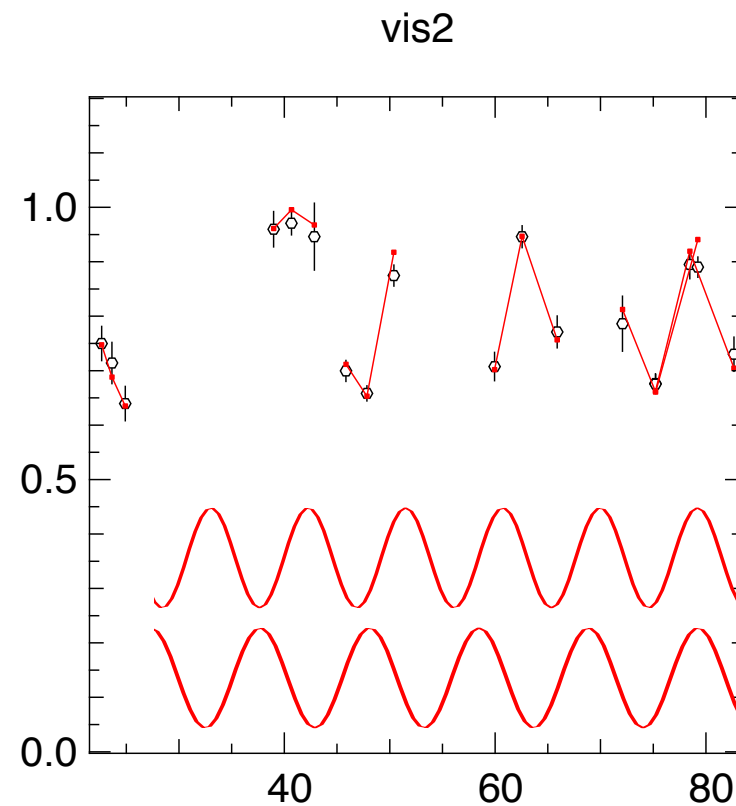
# Unambiguous FOV: (I) multiple solutions

V661\_CAR (2013-01-25)

$$V = \frac{1 + r e^{-2i\pi \frac{\vec{B}}{\lambda} \vec{\rho}}}{1 + r}$$

Did not find a clever way to quantify it :-)

Need long baseline for accurate astrometry.  
Need short baseline for “unicity” of the solution.



V661\_CAR  
mjd=56317.189

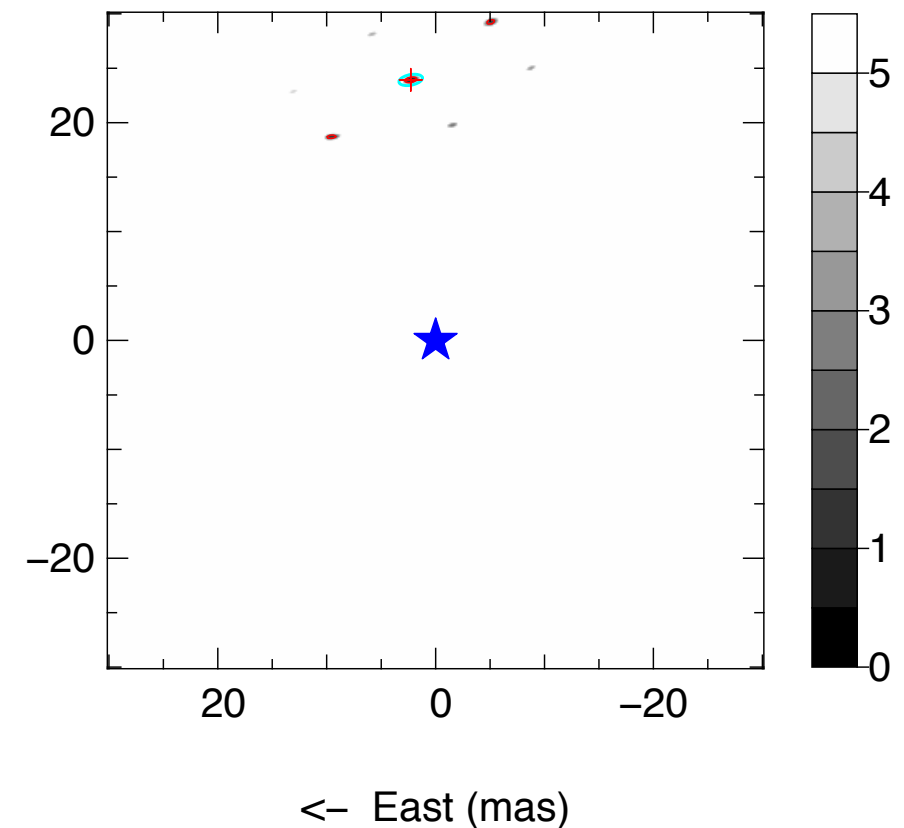
min(chi2)=1.0  
r=0.12\*

dE=2.29mas\*  
dN=23.93mas\*

$\rho=24.04\text{mas}$   
 $\theta=5.5\text{deg}$   
 $\varepsilon=\{1.09\text{mas}, 0.48\text{mas}, 101\text{deg}\}$

2013-01-24\_SCI\_V661\_CAR\_oiDataCalib

North (mas)  $\uparrow$



# Smearing: (I) loss of V2 at high baseline

HD156738 (2012-06-11)

Monochromatic:

$$V = \frac{1 + r e^{-2i\pi \frac{\vec{B}}{\lambda} \vec{\rho}}}{1 + r}$$

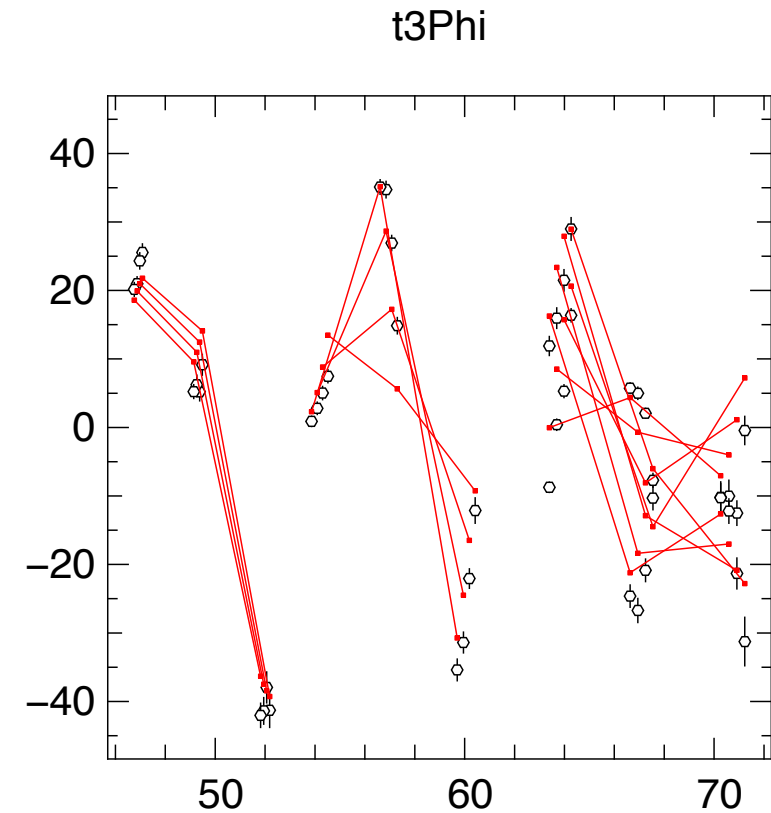
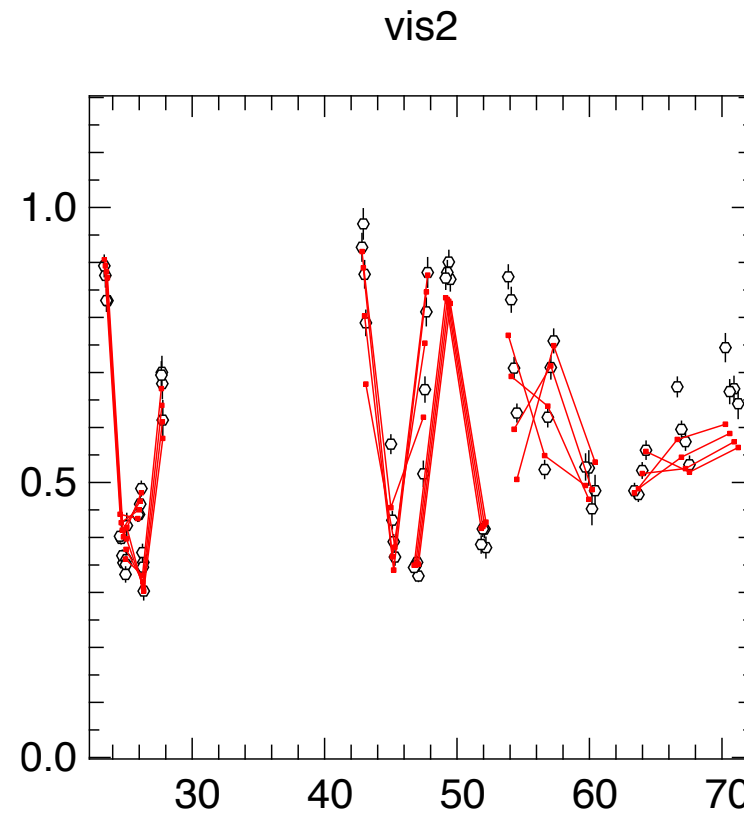
Large-band:

$$V = \int_{\lambda_0 - \Delta\lambda}^{\lambda_0 + \Delta\lambda} \frac{1 + r e^{-2i\pi \frac{\vec{B}}{\lambda} \vec{\rho}}}{1 + r} d\lambda$$

Approximate formula:

$$V \propto 1 + r e^{-2i\pi \frac{\vec{B}}{\lambda_0} \vec{\rho}} \text{sinc}\left(\pi \frac{\vec{B}}{R \cdot \lambda_0} \vec{\rho}\right)$$

$$R = \frac{\lambda_0}{\Delta\lambda}$$



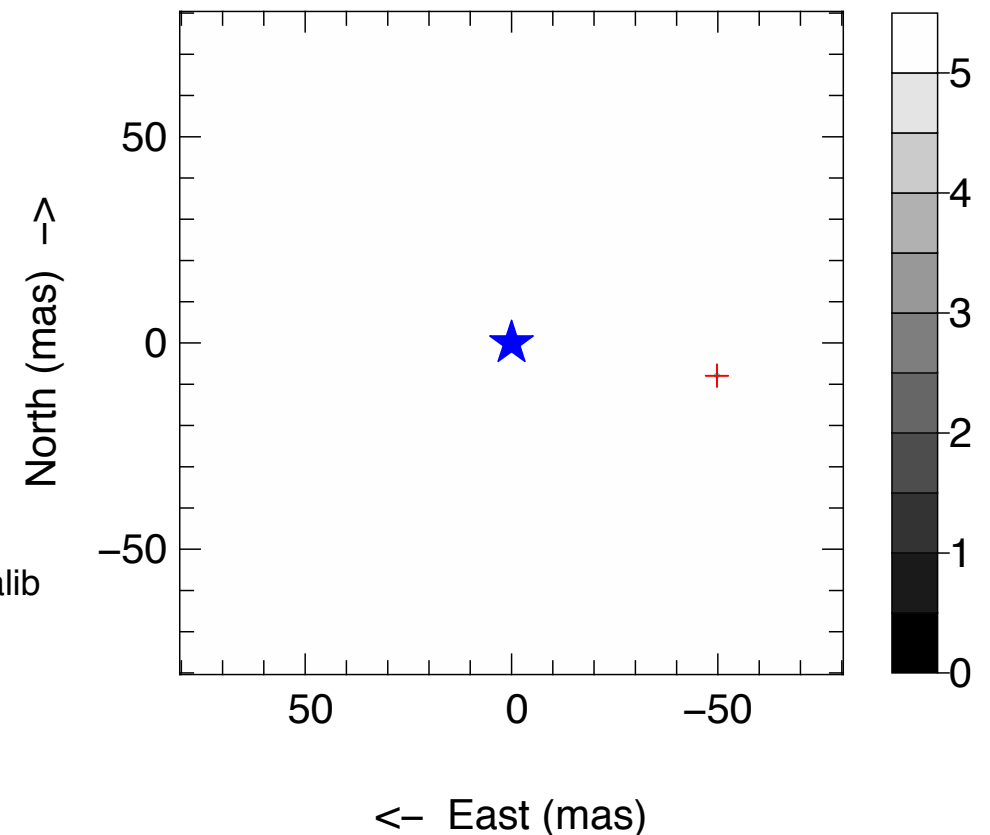
HD156738  
mjd=56089.285

min(chi2)=19.6  
r=0.31\*

dE=-49.75mas\*  
dN=-7.90mas\*

$\rho=50.38\text{mas}$   
 $\theta=-99.0\text{deg}$   
 $\varepsilon=\{0.33\text{mas}, 0.31\text{mas}, 105\text{deg}\}$

2012-06-10\_SCI\_HD156738\_oiDataCalib



# Smearing: (2) extreme case = flat V2

HD155889 (2012-06-11)

Monochromatic:

$$V = \frac{1 + r e^{-2i\pi \frac{\vec{B}}{\lambda} \vec{\rho}}}{1 + r}$$

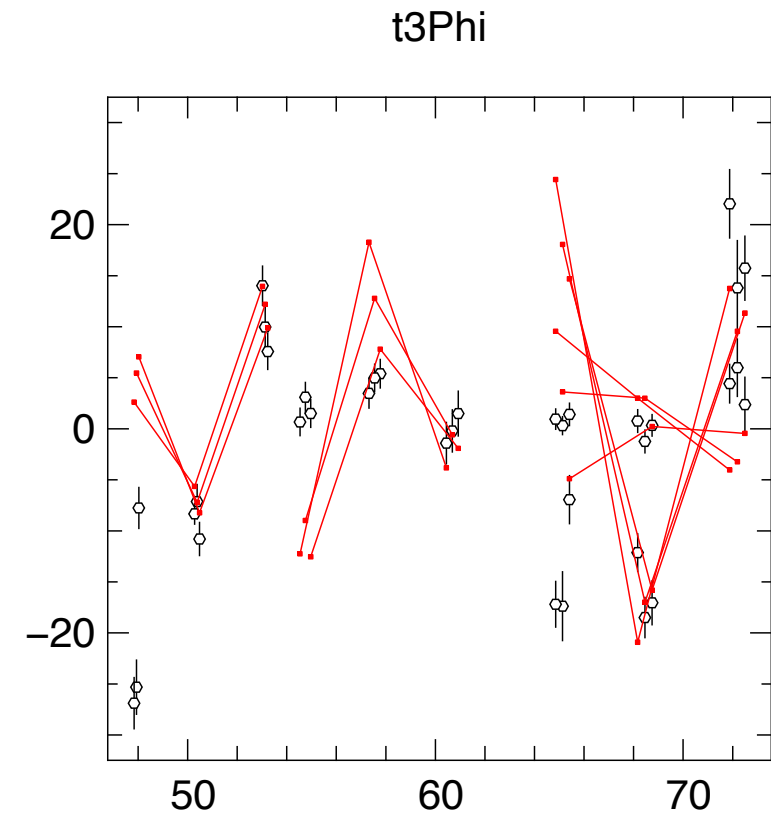
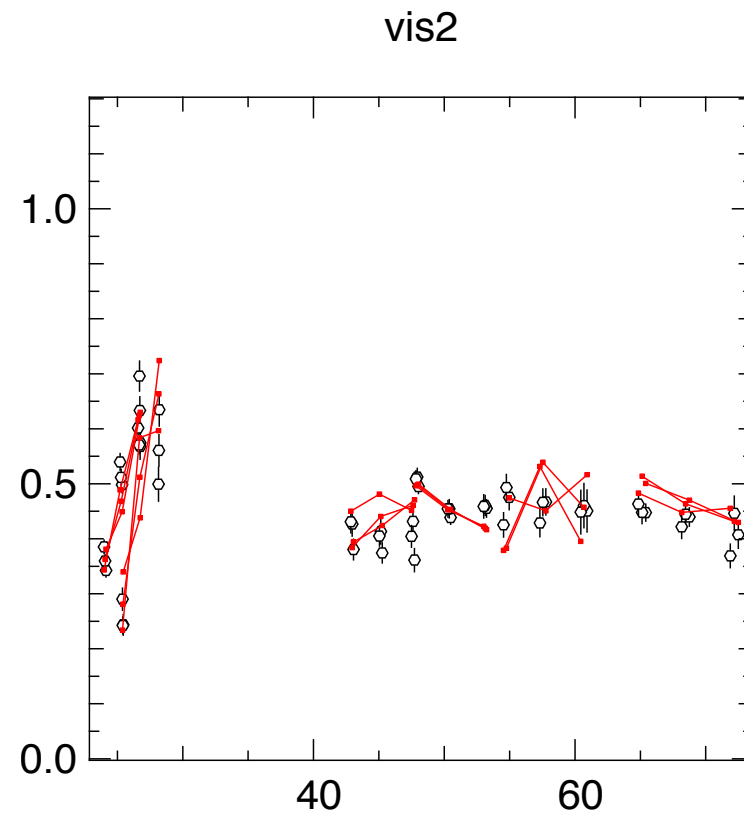
Large-band:

$$V = \int_{\lambda_0 - \Delta\lambda}^{\lambda_0 + \Delta\lambda} \frac{1 + r e^{-2i\pi \frac{\vec{B}}{\lambda} \vec{\rho}}}{1 + r} d\lambda$$

Approximate formula:

$$V \propto 1 + r e^{-2i\pi \frac{\vec{B}}{\lambda_0} \vec{\rho}} \text{sinc}\left(\pi \frac{\vec{B}}{R \cdot \lambda_0} \vec{\rho}\right)$$

$$R = \frac{\lambda_0}{\Delta\lambda}$$



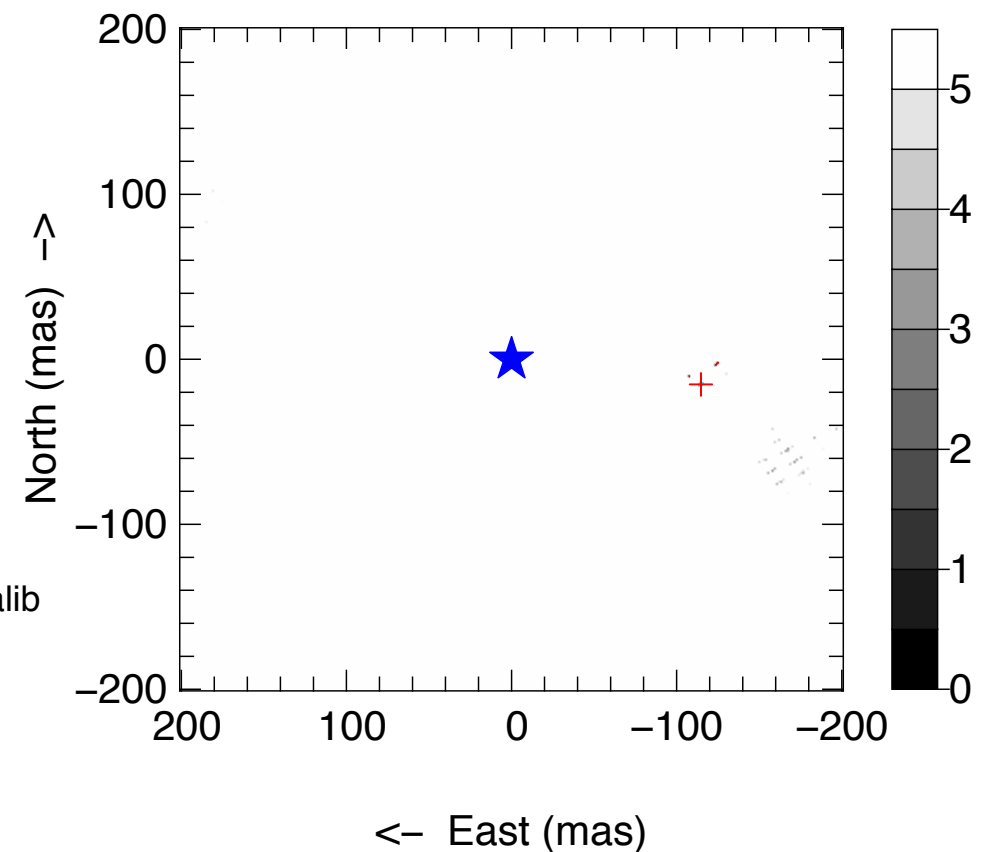
HD155889  
mjd=56089.275

min(chi2)=13.4  
r=0.48\*

dE=-114.72mas\*  
dN=-15.23mas\*

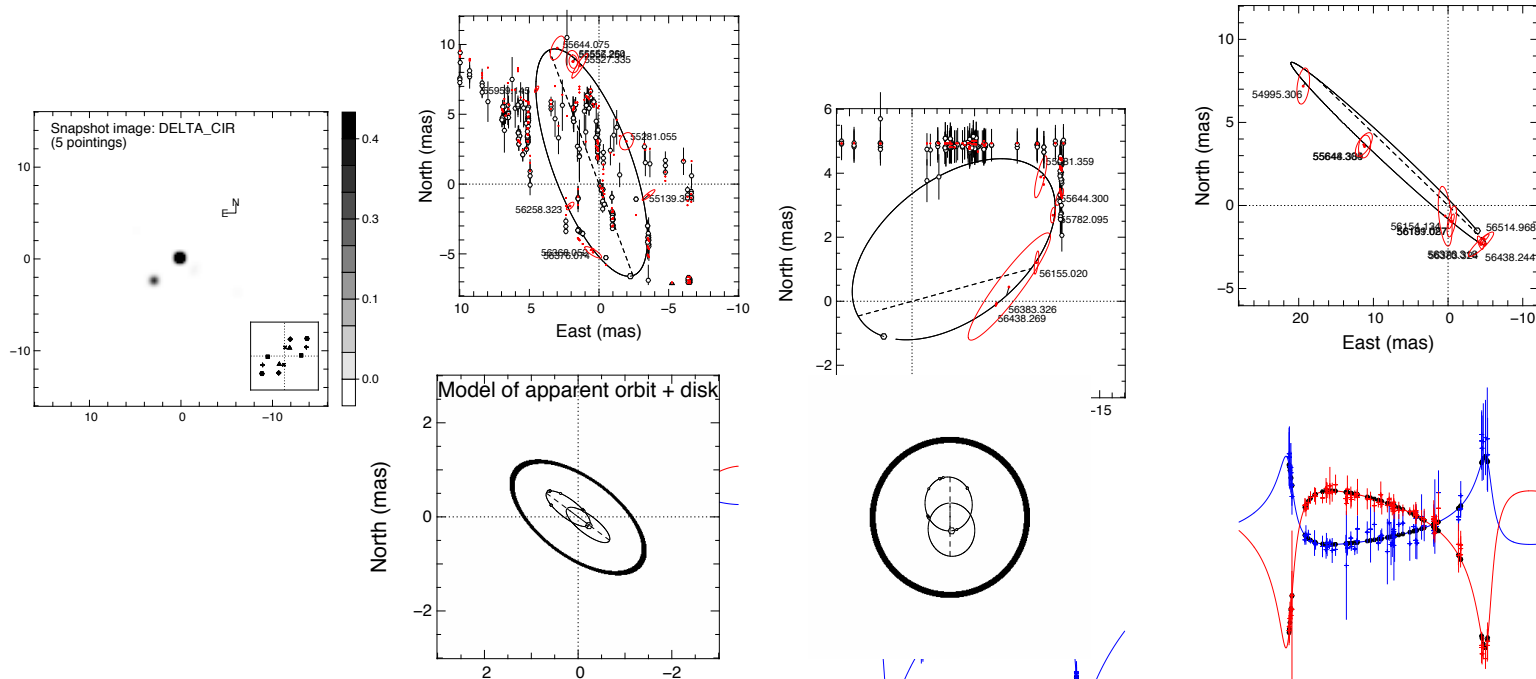
$\rho=115.72\text{mas}$   
 $\theta=-97.6\text{deg}$   
 $\varepsilon=\{1.00\text{mas}, 0.43\text{mas}, 131\text{deg}\}$

2012-06-10\_SCI\_HD155889\_oiDataCalib



# Some concluding words... what you should remember

It does work:



Some programs could be nice “backup fillers”:

- Very simple signal, easy to check for self-consistency = robust to calibration = good for bad conditions
- Short pointing are useful (at least with 3+ telescopes)
- But easy programs generally need long baselines

But several aspects of observational interferometry should not be overlooked...

- **Use existing tools.**
- **Read papers to know how to do things**
- **Collaborate with people.**



*Wish you all “nice fringes”...*